

MUM: flexible precise Monte Carlo algorithm for muon propagation through thick layers of matter

Igor A. Sokalski, Edgar V. Bugaev, Sergey I. Klimushin

Institute for Nuclear Research, Russian Academy of Science, 60th October Anniversary prospect 7a, Moscow 117312, Russia
(October 25, 2018)

We present a new Monte Carlo muon propagation algorithm MUM (MUons+Medium) which possesses some advantages over analogous algorithms presently in use. The most important features of algorithm are described. Results on the test for accuracy of treatment the muon energy loss with MUM are presented and analyzed. It is evaluated to be of 2×10^{-3} or better, depending upon simulation parameters. Contributions of different simplifications which are applied at Monte Carlo muon transportation to the resulting error are considered and ranked. It is shown that when simulating muon propagation through medium it is quite enough to account only for fluctuations in radiative energy loss with fraction of energy lost being as large as $0.05 \div 0.1$. Selected results obtained with MUM are given and compared with ones from other algorithms.

PACS number(s): 13.85Tp, 96.40.Tv, 02.70Lq

I. INTRODUCTION

Muon propagation through thick layers of matter was in the scope of interest for a long time since the first underground experiments with natural muon and neutrino fluxes had started. Development of “underground” technique has led to creation of number of underground, underwater and under-ice detectors by which a wide spectrum of problems is presently under investigation. Accurate calculation of muon transport plays an important role for such experiments because (a) neutrinos are detected by muons which are born in νN interactions and propagate a distance in medium from the point of interaction to a detector; (b) muons which are produced in atmospheric showers generated by cosmic rays represent the principal background for neutrino signal and therefore their flux at large depths should be well known; (c) atmospheric muons deep under sea or earth surface are the only intensive and more or less known natural calibration source which allows to confirm correctness of the detector model by comparison experimental and expected detector response; (d) flux of atmospheric muons itself carries the physical information which is of interest.

Along with analytical and semi-analytical methods (Refs. [1–13]) one widely uses Monte Carlo (MC) technique (Refs. [14–25]) which directly accounts for the stochastic nature of muon energy losses to simulate the muon propagation through matter. There are several MC muon transportation algorithms currently in use (see, e.g. Ref. [26] for detailed analysis of their advantages and disadvantages), but essential theoretical and experimental progress of last years makes to create new ones. Here we present a MC muon propagation code MUM (MUons+Medium) written in FORTRAN which possesses some advantages in accuracy and flexibility over analogous simulation algorithms (although it does not contain some important features in its current version, e.g. it does not give the 3D information about angular and lateral deviations of muons). The algorithm has been developed for the Baikal deep underwater neutrino experiment (Ref. [27]) but we believe it to be useful also for other experiments with natural fluxes of high energy muons and neutrinos. When working on MUM we aimed at creation of an algorithm which would:

- (a) account for the most recent corrections for the muon cross sections;
- (b) be of adequate and known accuracy, i.e. does not contribute an additional systematic error which would exceed one from “insurmountable” uncertainties (e.g. with muon and neutrino spectra and cross sections) and whose value would be well known for any setting of simulation parameters;
- (c) be flexible enough, i.e. could be optimized for each concrete purpose to desirable and well understood equilibrium between computation time and accuracy and be easily extended for any medium and any correction for the cross sections of the processes in which high energy muon loses its energy;
- (d) be “transparent”, i.e. provide user with the whole set of data related to used models for the muon cross sections;
- (e) be as fast as possible.

We describe the main features of our algorithm in Sec. II. Sec. III gives an analysis for the algorithm accuracy. In Sec. IV we report the results of investigation on the set of parameters which should be used to simulate the muon

propagation with an optimum equilibrium between accuracy and computation time. Sec. V presents selected results obtained with MUM in comparison with ones from other muon propagation MC codes, namely PROPMU (Ref. [22]) and MUSIC (Ref. [24]). Sec. VI gives general conclusions. We also present parameterizations for muon cross sections as they are used in MUM in Appendix A and give proof of formula for free path between two muon interactions, as treated in our algorithm, in Appendix B.

II. ALGORITHM DESCRIPTION

The basic features of the MUM algorithm are as follows.

- (a) The code does not use any preliminary computed data as an input, all necessary tables are prepared at the stage of initiation on the base of five relatively short routines, four of which return differential cross sections $d\sigma(E, v)/dv$ (where E is muon energy, v is fraction of energy lost $v = \Delta E/E$) for bremsstrahlung, direct e^+e^- -pair production, photo-nuclear interaction and knock-on electron production, correspondingly, and fifth one does stopping power due to ionization $[dE(E)/dx]_{ion}$ (see Appendix A for corresponding formulas). Thus, it is easy for any user to correct or even entirely change the model for muon interactions as it is necessary. Also any material can be easily composed. Three media, namely pure water, ice and standard rock are available directly.
- (b) We have tried to decrease the “methodical” part of systematic error which originates from finite accuracy of numerical procedures on interpolation, integration, etc., down to as low level as possible, special attention was put on procedures which simulate free path between two sequential muon interactions and fraction of energy lost. To combine this with the high speed of simulation the values for free paths, energy losses, differential and total cross sections along with solutions for all ordinary and integral equations are computed in MUM at the initiation stage, tabulated and then referenced when necessary with an interpolation algorithm whose accuracy has been carefully tested for each table by comparison with directly computed values to be not worse than 0.5% (typically, much better).
- (c) The most important parameters are changeable and can be tuned to an optimum combination, depending upon desirable accuracy, necessary statistics and restriction on the computation time for each concrete problem.
- (d) The code combines algorithms for muon transportation through thick layers of matter down to detector and for simulation muon interactions within detector sensitive volume (these algorithms have to differ from each other). This is important for deep underwater and under-ice Cherenkov neutrino telescopes (see Refs. [27–30]), where the same material (water or ice) represents both a shield which absorbs atmospheric muons and detecting medium in which muons and shower particles resulting from muon interactions generate Cherenkov photons detected by phototubes.
- (e) Formally, initial muon energies up to 1 EeV can be processed by the MUM algorithm but uncertainties with muon cross sections which grows along with the muon energy (especially, for photo-nuclear interaction) make one to apply MUM output with care at muon energies $E > 0.1 \div 1$ PeV. Landau-Pomeranchuk-Migdal effect is not accounted in MUM.
- (f) Besides muon transportation algorithm itself, the code includes number of routines which allows to obtain directly values for differential and total cross sections, mean free paths, energy losses and other related data for the given set of input parameters. Sampling the atmospheric muon energies at the sea level according to different models for spectrum is possible with MUM, as well. Also several test procedures are included which provide by data concerning accuracy of different algorithm steps. See Sec. III, Sec. IV and Sec. V for selected output of these procedures.

The usual approximation for treatment the muon energy loss is applied in the MUM algorithm: muon interactions with comparatively large energy transfers when fraction of energy lost v exceeds some value v_{cut} , are accounted by direct simulation of $v \geq v_{cut}$ for each single interaction according to shape of differential cross sections (these interactions lead to “stochastic” energy loss or SEL) while the part of interaction with relatively small v is treated by the approximate concept of “continuous” energy loss (CEL) using the stopping power formula

$$\left[\frac{dE}{dx}(E) \right]_{CEL} = \frac{N_A}{A_{eff}} \rho E \sum_{j=b,p,n} \sum_{i=1}^n \left[k_i \int_{v_{min}^{i,j}}^{v_{cut}} \frac{d\sigma_i^j(E, v)}{dv} v dv \right]$$

$$+ \left[\frac{dE}{dx}(E) \right]_{ion} - \frac{N_A}{A_{eff}} \rho E \sum_{i=1}^n \left[k_i \int_{v_{cut}}^{v_{max}^{i,e}} \frac{d\sigma_i^e(E, v)}{dv} v dv \right]. \quad (2.1)$$

Here index j indicates type of interaction ($j = b$ for bremsstrahlung, $j = p$ for direct e^+e^- -pair production, $j = n$ for photo-nuclear interaction and $j = e$ for knock-on electron production, respectively); index i runs over n kinds of atoms given material consists of; $k_i = N_i/N_{tot}$ is fraction of i -th element; N_i and N_{tot} are number of given kind of atoms and total number of atoms, respectively, per unit of material volume; N_A is the Avogadro number; ρ is the material density; $A_{eff} = N_{tot}^{-1} \sum_{i=1}^n (N_i A_i)$ is an effective atomic weight for given material; A_i is atomic weight for i -th element; $v_{min}^{i,j}$ is minimum kinematically allowed fraction of energy lost for i -th element at j -th process. One is forced to decompose energy losses into two parts because simulation of all interactions with $v \geq v_{min}$ would result in infinite computation time due to steep dependence of muon cross sections on v : they decrease with v at least as $d\sigma(E, v)/dv \propto v^{-1}$ and for some processes are not finite at $v \rightarrow 0$. Number of interactions to be simulated per unit of muon path grows, roughly, as $N_{int} \propto v_{cut}^{-1}$ along with computation time. Actually, two different criteria by which the given muon interaction is attributed either to SEL or to CEL are available in the frame of the MUM algorithm. The first one (relative) has been described above and is applied when muon is transported down to detector location. Second, absolute criterium, is useful when simulating muon interactions within an underwater or under-ice array to obtain the detector response with the fixed energy threshold: interaction is of SEL type if $\Delta E \geq \Delta E_{cut}$ and of CEL type, if $\Delta E < \Delta E_{cut}$. Optionally, cross section for knock-on electron production $d\sigma^e(E, v)/dv$ can be set in MUM to zero, in which case muon propagation down to detector is simulated with entirely “continuous” ionization and its fluctuations are neglected but simulation of the muon interactions with fixed energy threshold includes knock-on electron production in any case. Both v_{cut} and ΔE_{cut} represent parameters for MUM initiation procedure and can be set to any values within $10^{-4} \leq v_{cut} \leq 0.2$ and $10 \text{ MeV} \leq \Delta E_{cut} \leq 500 \text{ MeV}$, correspondingly. The optimum value for ΔE_{cut} depends upon configuration of the given detector and also upon characteristics of algorithms which simulate the shower development, the Cherenkov photons generation and propagation, and detector response. All this is out of given article scope, therefore we discuss this parameter nowhere below except for mentioning that Eqs. (2.1), (2.3) and (2.6) are used in algorithm with absolute treatment of the muon energy loss decomposition being modified by replacement $v_{cut} \rightarrow \Delta E_{cut}/E$. Influence of simplified entirely “continuous” treatment of ionization and value of v_{cut} upon simulation accuracy is analyzed in details in Sec. IV (see also Ref. [31]).

The principal steps of simulation are as follows.

I. For muon with initial energy E_1 the free path L till interaction with $v \geq v_{cut}$ is simulated. For this, after a random number η uniformly distributed in a range from 0 to 1 has been sampled, one solves the following set of equations:

$$\begin{cases} -\ln(\eta) = \int_{E_2}^{E_1} [(dE(E)/dx)_{CEL} \bar{L}(E)]^{-1} dE \\ L = \int_{E_2}^{E_1} [(dE(E)/dx)_{CEL}]^{-1} dE \end{cases} \quad (2.2)$$

(proof of Eqs. (2.2) is given in Appendix B). Here, $E_2 < E_1$ is muon energy at the point of interaction and energy dependent mean free path $\bar{L}(E)$ between two interactions with fraction of energy lost $v \geq v_{cut}$ is expressed by

$$\bar{L}(E) = \frac{A_{eff}}{\rho N_A} \left\{ \sum_{j=b,p,n,e} \sum_{i=1}^n \left[k_i \int_{v_{cut}}^{v_{max}^{i,j}} \frac{d\sigma_i^j(E, v)}{dv} dv \right] \right\}^{-1}, \quad (2.3)$$

where $v_{max}^{i,j}$ is maximum kinematically allowed fraction of energy lost for i -th element at j -th kind of interaction. First equation in Eqs. (2.2) is solved for variable E_2 , then free path L can be found by second equation. We would like to stress that such approach allows to perform the accurate simulation independently on chosen value of v_{cut} in contrast to commonly used simplification

$$L_{approx} = -\bar{L}(E_1) \ln(\eta), \quad (2.4)$$

which neglects dependence $\bar{L}(E)$ upon energy and, consequently is (a) the less accurate the larger v_{cut} is and (b) produces the error of different signs for the cases when ionization is included in SEL or its fluctuations are neglected.

It is illustrated by two plots in Fig. 1. Upper plot shows function $\bar{L}(E)$ for pure water. Two sets of curves are presented for two models of ionization. Each set includes dependencies for 3 values of v_{cut} : 10^{-4} , 10^{-3} and 10^{-2} . In fact, $\bar{L}(E)$ is almost a constant at $E > 5$ TeV but changes steeply at lower energies. It increases with decrease of energy if ionization is entirely “continuous” and, on the contrary, it decreases if ionization is included in SEL. Thus, simulating free path by Eq. (2.4) one overestimates it (and consequently underestimates energy loss) in case when ionization is included in SEL and, on the contrary one underestimates free path and overestimates energy loss in case of completely “continuous” ionization. Lower plot in Fig. 1 shows resulting error in the value of simulated free path if $-\ln(\eta) = 1$ (for larger $-\ln(\eta)$ the effect is more significant). The set of curves represent dependencies $k(E) = L_{approx}(E)/L(E)$ with $L(E)$ computed by Eqs. (2.2) and $L_{approx}(E)$ computed by Eq. (2.4). With ionization included in SEL overestimation for free path is less than 1% at $v_{cut} \leq 10^{-3}$ but reaches $\sim 15\%$ at $v_{cut} = 10^{-2}$ which leads to $1 \div 2\%$ underestimation of total energy loss below muon energy 1 TeV. In case with “continuous” ionization the effect is of opposite sign and again is more significant for large v_{cut} .

II. After free path L and muon energy E_2 have been found from Eqs. (2.2), the type of interaction is simulated according to proportion between total cross sections of different processes:

$$\sigma^b : \sigma^p : \sigma^n : \sigma^e \quad (2.5)$$

which are computed as:

$$\sigma^j = \sum_{i=1}^n \left[k_i \int_{v_{cut}}^{v_{i,j}^{max}} \frac{d\sigma_i^j(E_2, v)}{dv} dv \right]. \quad (2.6)$$

III. Fraction of energy lost v is simulated according to shape of differential cross section for given process j :

$$\frac{d\sigma^j}{dv}(E_2, v) = \sum_{i=1}^n k_i \frac{d\sigma_i^j}{dv}(E_2, v) \quad (2.7)$$

and new muon energy $E'_1 = E_2 \cdot (1 - v)$ is determined.

IV. Steps I–III are repeated sequentially until muon either reaches the level of observation or stops. Muon are considered as stopped as soon as its energy decreases down to 0.16 GeV which corresponds to the Cherenkov threshold for muon in pure water.

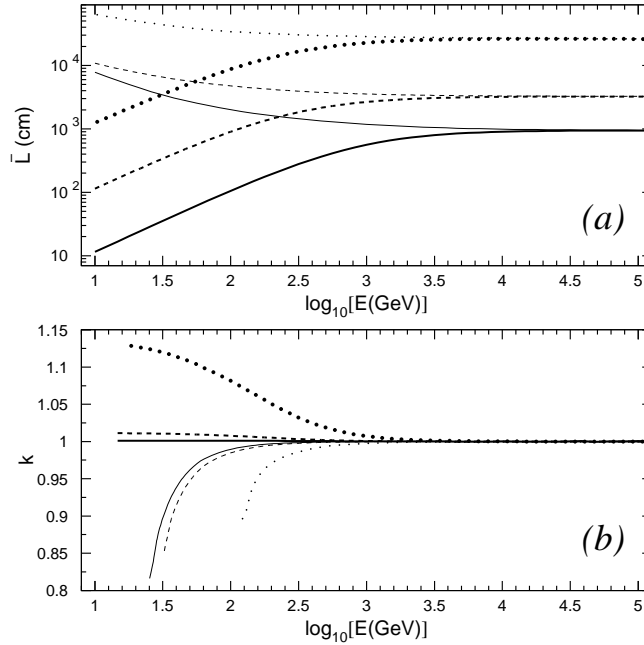


FIG. 1. (a) - mean free path between two sequential muon interactions with fraction of energy lost $v > v_{cut}$ $\bar{L}(E)$ (Eq. (2.3)) in pure water vs. muon energy. Two sets of curves correspond to two models of ionization. Thick lines are for ionization included in SEL, thin ones correspond to entirely “continuous” ionization. Solid lines: $v_{cut} = 10^{-4}$; dashed lines: $v_{cut} = 10^{-3}$; dotted lines: $v_{cut} = 10^{-2}$. (b) - Function $k(E) = L_{approx}(E)/L(E)$ for $-\ln(\eta) = 1$ (see text). Thickness and type of lines are of the same meaning as for plot (a).

III. ALGORITHM ACCURACY

As described in Sec. II the MUM code (as well as any muon MC propagation algorithm) consists of the set of procedures on numerical solution of equations, interpolation and integration. All these procedures are of finite accuracy and, consequently, the incoming model for muon energy loss is somewhat corrupted by them. Thus, resulting energy loss as it *simulated* by a code are not the same as energy loss as it can be calculated by *integration* the differential cross sections which are at the input of the same code. The difference between simulated and calculated energy loss contains errors which are contributed by each step of simulation algorithm and thus, is a good quantitative criterium for its *inner accuracy*, whose contribution to the resulting error must not exceed one which comes, e.g. from uncertainties with muons cross sections and medium composition. Therefore to demonstrate accuracy of presented algorithm we have chosen just data on the relative difference $(L_s - L_i)/L_i$ between simulated L_s and integrated L_i total muon energy loss as was obtained with MUM for the pure water (Fig. 2) and standard rock ($\rho = 2.65 \text{ g cm}^{-3}$, $A = 22$, $Z = 11$, Fig. 3). Inner accuracy is presented in the figure as a function of muon energy for several values of v_{cut} and two models of ionization energy loss. Values of L_s were obtained as follows. For each muon energy E_1 a distance D was chosen and propagation of $N = 4 \times 10^6$ muons over this distance was simulated. The condition $N \cdot D \gg \bar{L}(E_1)$ must be obeyed to obtain statistically significant result but, at the same time, D should be short enough to be passed by muons without decrease their energy down to zero, which practically leads to $D = 0.5 \text{ m} \div 300 \text{ m}$ depending upon muon energy, value of v_{cut} and kind of medium. For each i -th muon its final energy E_2^i was fixed and then L_s was calculated as

$$L_s = \frac{1}{D} \left(E_1 - \frac{1}{N} \sum_{i=1}^N E_2^i \right). \quad (3.1)$$

L_i was computed as

$$L_i = \frac{1}{D} (E_1 - E_2), \quad (3.2)$$

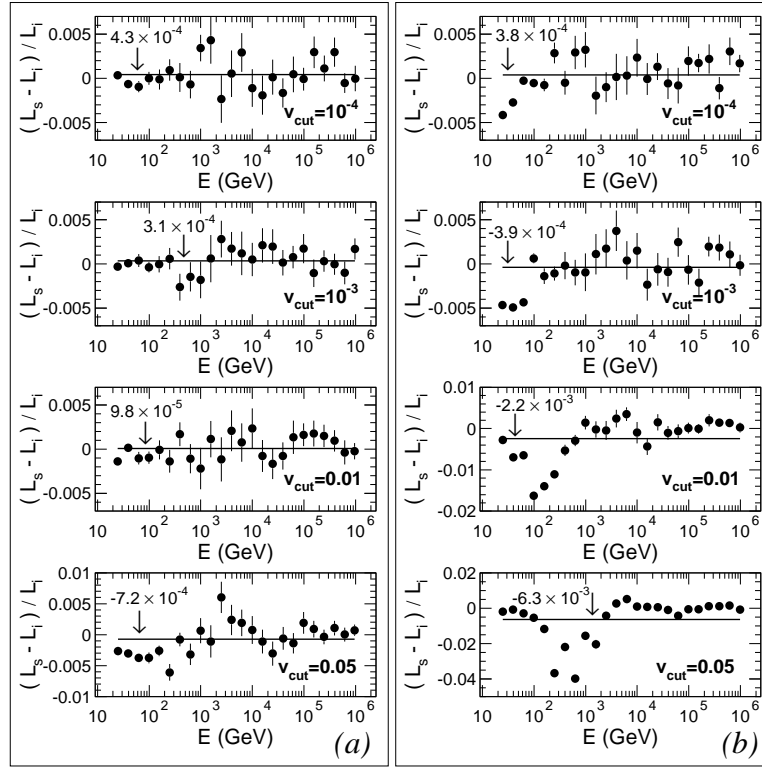


FIG. 2. Relative difference $(L_s - L_i)/L_i$ between “simulated” L_s (Eq. (3.1)) and “integrated” L_i (Eqs. (3.2), (3.3)) total muon energy loss in the pure water. Horizontal solid line on each plot shows averaged over 24 tested muon energies value for $(L_s - L_i)/L_i$ which, additionally, is given at the upper left corner by the figure. Statistical error at 1σ -level is shown at each point. (a) - ionization is included in SEL; (b) - ionization is entirely “continuous”.

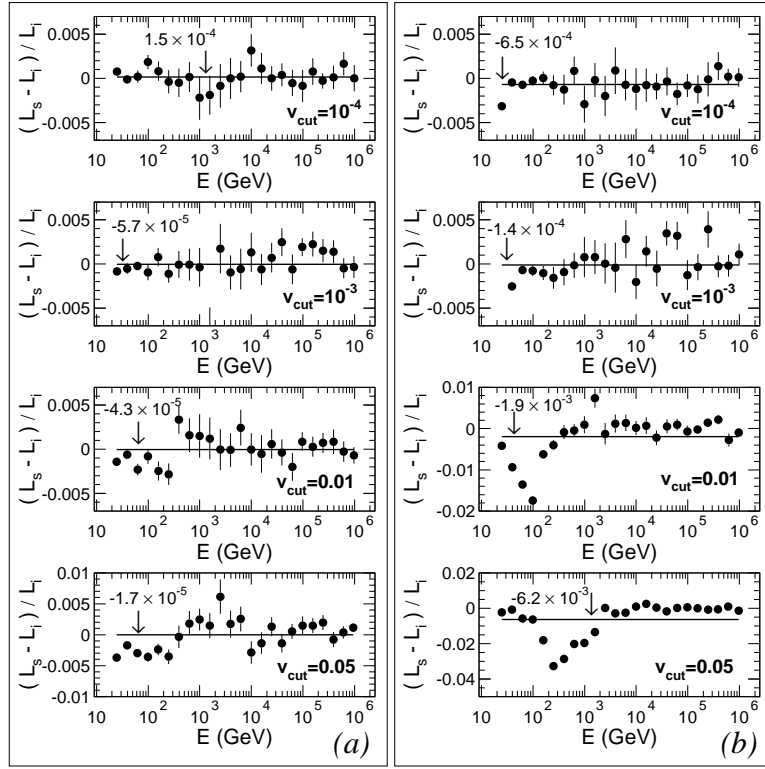


FIG. 3. The same as in Fig. 2 for standard rock ($\rho = 2.65 \text{ g cm}^{-3}$, $A = 22$, $Z = 11$).

where E_2 was found as a solution of integral equation for the muon range:

$$D = \int_{E_2}^{E_1} \left\{ \frac{N_A}{A_{eff}} \rho E \sum_{j=b,p,n} \sum_{i=1}^n \left[k_i \int_{v_{min}^{i,j}}^{v_{max}^{i,j}} \frac{d\sigma_i^j(E, v)}{dv} v dv \right] + \left[\frac{dE}{dx}(E) \right]_{ion} \right\}^{-1} dE. \quad (3.3)$$

Horizontal solid line on each plot shows the value for $(L_s - L_i)/L_i$ averaged over 24 tested muon energies which, additionally, is given at upper left corner by a figure. Fig. 2(a) and Fig. 3(a) indicate an excellent inner accuracy of the MUM algorithm with ionization included in SEL both for water and standard rock. Up to $v_{cut} = 5 \times 10^{-2}$ all points are within 0.6%-deviations which, besides, are of both signs, so averaged accuracy remains better than 10^{-3} . Fig. 2(b) and Fig. 3(b) (which correspond to simplified completely “continuous” ionization) shows somewhat worse accuracy of the algorithm which falls down when v_{cut} increases. Accuracy was found to be within 1% (with except for few points around muon energy $E = 100 \text{ GeV}$) up to $v_{cut} = 10^{-2}$ with averaged accuracy within 2×10^{-3} . This last value may be used as a conservative evaluation of inner accuracy for the MUM algorithm. Statistically significant likeness of plots obtained for water and standard rock can be seen.

Thus, we conclude that assuming an optimistic evaluation of 1% for uncertainties in muon cross sections (Refs. [26,32]) the inner inaccuracy of MUM does not exceed them for any $v_{cut} \leq 5 \times 10^{-2}$ if ionization is included in SEL and for any $v_{cut} \leq 10^{-2}$ if ionization is treated as entirely “continuous process”, independently upon material.

IV. THE OPTIMUM SETTING OF SIMULATION PARAMETERS

As was described in Sec. II v_{cut} is a parameter in the MUM algorithm and can be set optionally to different values. The larger is v_{cut} the higher is the speed of simulation, because the less muon interactions have to be simulated per unit of the muon path. But, on the other hand, too large value of v_{cut} leads to the lost of accuracy since some essential part of fluctuations in the muon energy losses comes out of direct simulation. Thus, the question is *how large value of v_{cut} may be chosen to keep result within desirable accuracy?* Also different models for ionization can be used: it can be optionally either treated as completely “continuous” process or included in SEL. Small energy transfers strongly dominate at knock-on electron production ($d\sigma^e(E, v)/dv \propto v^{-2}$), so this process is almost non-stochastic and it seems to be reasonable to exclude knock-on electrons from simulation procedure when simulating SEL which saves

computation time noticeable. *How much does it affect the result of simulation?* Influence of these factors on simulated result had been discussed in literature (see, e.g. Refs. [12,22,24,25]) but in our opinion more detailed analysis was lacking. Therefore we have undertaken our own investigation which is reported in this Section. For that we performed several sets of simulations both for propagation of mono-energetic muon beams and atmospheric muons sampled by sea level spectrum (in the later case we limited ourselves by simulation only vertical muons) through pure water down to depths from $D = 1$ km to $D = 40$ km. Of course, distances of more than several kilometers for vertical muons do not concern any real detector but simulations for large depths allow us to study general regularities which correspond, e.g. to nearly horizontal directions. Several runs were done for standard rock, as well. We tested different settings of parameters which were as follows.

- (a) v_{cut} , which changed within a range of $10^{-4} \leq v_{cut} \leq 0.2$. Inner accuracy of the MUM code becomes somewhat worse at $v_{cut} \geq 5 \times 10^{-2}$, especially if fluctuations in ionization are not simulated (Sec. III) therefore results for $v_{cut} = 0.1$ and $v_{cut} = 0.2$ are presented here only to illustrate some general qualitative regularities.
- (b) Model for ionization.
- (c) Parameterization for vertical sea level atmospheric muon spectrum. Two spectra were tested, namely one proposed in Ref. [33] (basic):

$$\frac{dN}{dE} = \frac{0.175 E^{-2.72}}{cm^2 s sr GeV} \left(\frac{1}{1 + E/103 GeV} + \frac{0.037}{1 + E/810 GeV} \right), \quad (4.1)$$

and the Gaisser spectrum (Ref. [34]):

$$\frac{dN}{dE} = \frac{0.14 E^{-2.7}}{cm^2 s sr GeV} \left(\frac{1}{1 + E/104.6 GeV} + \frac{0.054}{1 + E/772.7 GeV} \right). \quad (4.2)$$

- (d) Parameterization for total cross section for absorption of a real photon by a nucleon at photo-nuclear interaction $\sigma_{\gamma N}$ which was treated both according to the Bezrukov-Bugaev parameterization proposed in Ref. [35] (basic) and the ZEUS parameterization (Ref. [36]) (see. Appendix A 2 for formulas).
- (e) A factor k_{σ} which all muon cross sections along with stopping power due to ionization were multiplied by to test influence of uncertainties in muon cross sections (and, consequently, in energy losses) upon result. We applied $k_{\sigma} = 1.0$ as a basic value but set also $k_{\sigma} = 0.99$ and $k_{\sigma} = 1.01$, which corresponds to decrease and increase of total energy loss by 1%, respectively. Note that it is an “optimistic” evaluation, the real accuracy of existing parameterization for muon cross sections is worse (see Refs. [26,32]).

For each run we fixed the muon spectra at final and several interim depths. The differences between obtained spectra were a point of investigation.

At the first set of simulations we propagated mono-energetic muon beams of 4 fixed initial energies $E_s = 1$ TeV, 10 TeV, 100 TeV and 10 PeV down to slant depths $D = 3.2$ km, 12 km, 23 km and 40 km, respectively, through pure water. The value D for each initial muon energy was chosen so that majority of muons had been stopped after propagation the given distance. This allows to track differences in simulated results obtained with different settings of parameters for all segments of muon beam path. In each case propagation of 10^6 muons was simulated. Fig. 4 shows resulting survival probabilities $p = N_D/N_s$ (where $N_s = 10^6$ is initial number of muons and N_D is number of muons which have survived after propagation down to the slant depth D) vs. v_{cut} for final and five interim values of D . Two curves are given on each plot for two models of ionization. Also results for $k_{\sigma} = 1.00 \pm 0.01$ and for $\sigma_{\gamma N}$ parameterization according to Ref. ([36]) are presented as simulated with the most accurate value $v_{cut} = 10^{-4}$.

The following conclusions can be done.

- (a) In most cases except for some plots of the lower row and the left column in Fig. 4 (which corresponds to low survival probabilities and low muon initial energies, respectively) uncertainty in our knowledge of muon cross sections gives the principal effect which essentially exceeds ones from other tested parameters.
- (b) The difference between survival probabilities for two models of ionization is the less appreciable the larger muon energy is. It is quite understandable because at muon energies $E < 1$ TeV ionization represents the great bulk of total energy loss, and vice versa, it becomes minor at $E > 1$ TeV. Thus, contribution which is given by ionization at higher energies is small and, the more, its fluctuations do not play an important role. For muons with initial energies $E \gg 1$ TeV fluctuations in ionization become important only at very last part of muon path and “are not in time” to produce some noticeable effect.

- (c) Generally, parameterizations for $\sigma_{\gamma N}$ as proposed in Refs. [35,36] do not show a noticeable difference in terms of survival probabilities, in most cases it is within statistical error or exceeds it only slightly.
- (d) Increase of v_{cut} gives effect of both signs in survival probabilities: function $p(v_{cut})$ grows at the beginning of muon path and falls at the last part. The same “both-sign” dependencies are observed for ionization model.
- (e) For $v_{cut} \leq 0.05$ there is almost no dependence of survival probability on v_{cut} except for very last part of muon path where survival probability becomes small. Generally, dependence $p(v_{cut})$ is the less strong the larger initial muon energy is.

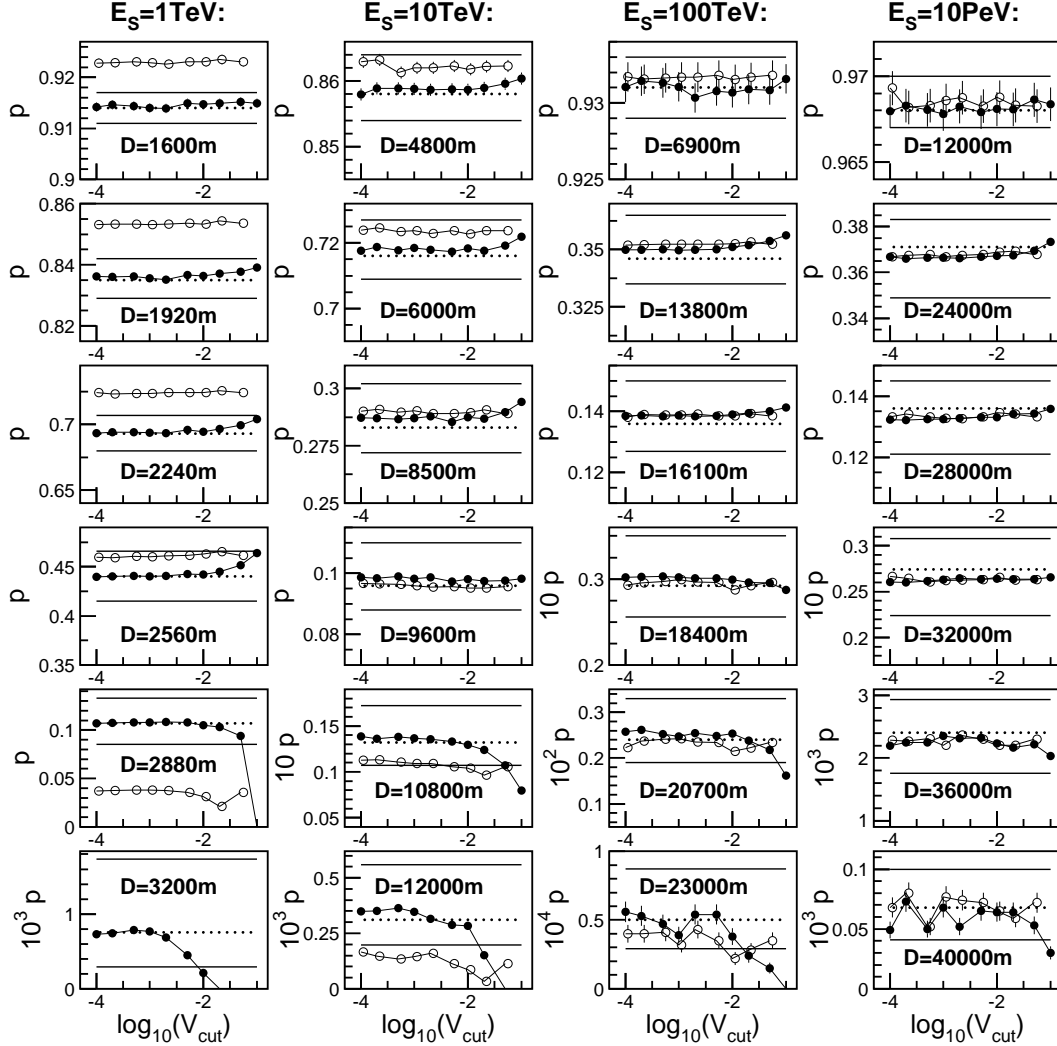


FIG. 4. Survival probabilities $p = N_D/N_s$ (where $N_s = 10^6$ is initial number of muons in the beam and N_D is number of muons which have survived after propagation down to slant depth D in pure water) vs. v_{cut} . Values of p were obtained as a result of simulation with MUM for mono-energetic muon beams with initial energies $E_s = 1$ TeV (1st column of plots), 10 TeV (2nd column), 100 TeV (3rd column) and 10 PeV (4th column). Each column contains six plots which correspond to six slant depths D (which differs for different E_s). Closed circles represent survival probabilities which were simulated with ionization energy losses included in SEL, open ones correspond to computation with completely “continuous” model of ionization. Two horizontal solid lines on each plot show the value for survival probability computed with all muon cross sections multiplied by a factor $k_\sigma = 1.01$ (lower line) and $k_\sigma = 0.99$ (upper line) for $v_{cut} = 10^{-4}$. Horizontal dotted lines correspond to $v_{cut} = 10^{-4}$ and cross section for absorption of a real photon at photo-nuclear interaction parameterized according to Ref. [36] instead of Ref. [35] which is basic in MUM. Note different scales at Y-axis.

The last item is illustrated complementary by Fig. 5 and Fig. 6 which show that for all initial energies E_s simulated survival probability does not depend, in fact, on v_{cut} until 90% (for $E_s = 1$ TeV) to 99.5% (for $E_s = 10$ PeV) muons have been stopped.

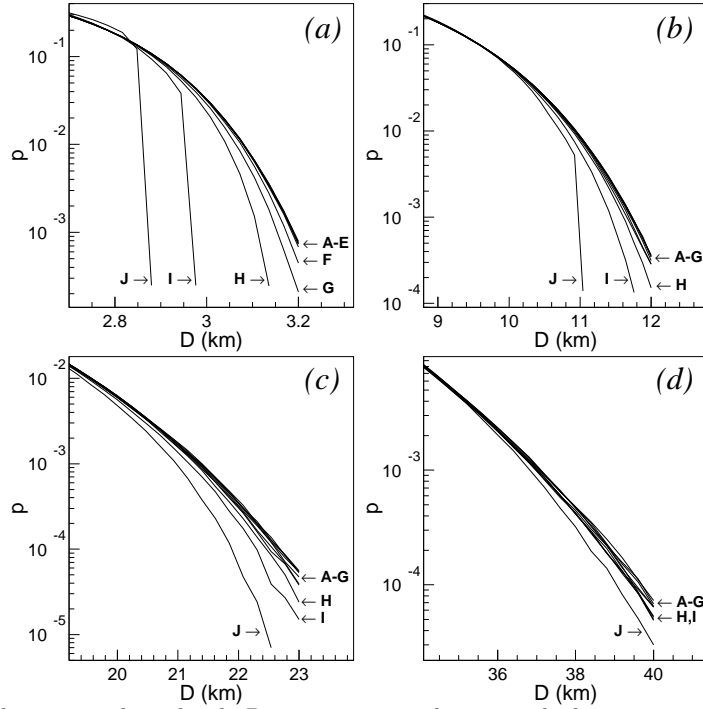


FIG. 5. Survival probability p vs. slant depth D in pure water down to which propagation of mono-energetic muon beam with initial energy $E_s = 1$ TeV (a), 10 TeV (b), 100 TeV (c) and 10 PeV (d) is simulated. On each plot 10 lettered curves which correspond to different values of v_{cut} are shown. Meaning of letters is as follows: A - $v_{cut} = 10^{-4}$, B - $v_{cut} = 2 \times 10^{-4}$, C - $v_{cut} = 5 \times 10^{-4}$, D - $v_{cut} = 10^{-3}$, E - $v_{cut} = 2 \times 10^{-3}$, F - $v_{cut} = 5 \times 10^{-3}$, G - $v_{cut} = 10^{-2}$, H - $v_{cut} = 2 \times 10^{-2}$, I - $v_{cut} = 5 \times 10^{-2}$, J - $v_{cut} = 10^{-1}$. This figure displays results which were obtained by simulation with ionization losses included in SEL. Statistical errors (which cause some un-smoothness of curves at small p) are not shown.

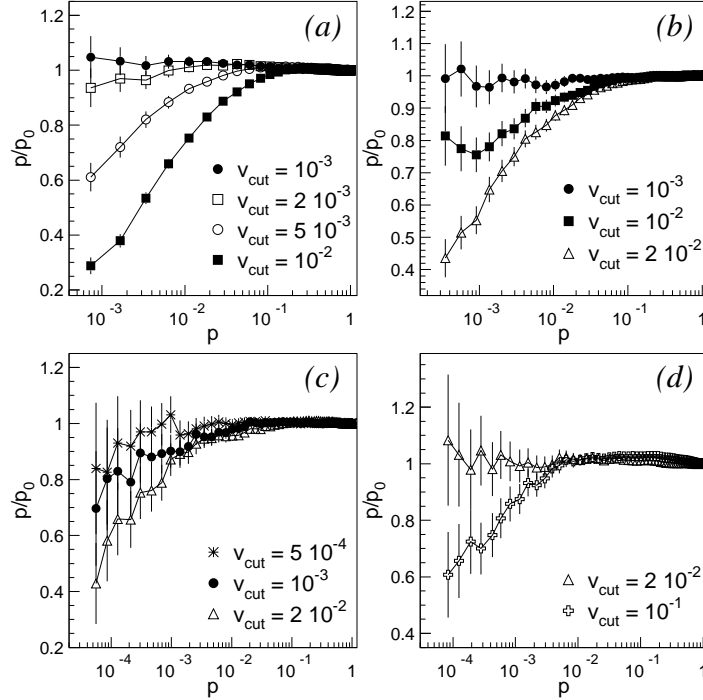


FIG. 6. Relation p/p_0 vs. p . p is survival probability for muon s of initial energy $E_s = 1$ TeV (a), 10 TeV (b), 100 TeV (c) and 10 PeV (d) at propagation through pure water with ionization included in SEL as simulated for different values of v_{cut} ; p_0 is survival probability simulated under the same conditions for $v_{cut} = 10^{-4}$. Difference in p/p_0 becomes noticeable only at $p < 10^{-1}$, i.e. at the very last part of muon beam path.

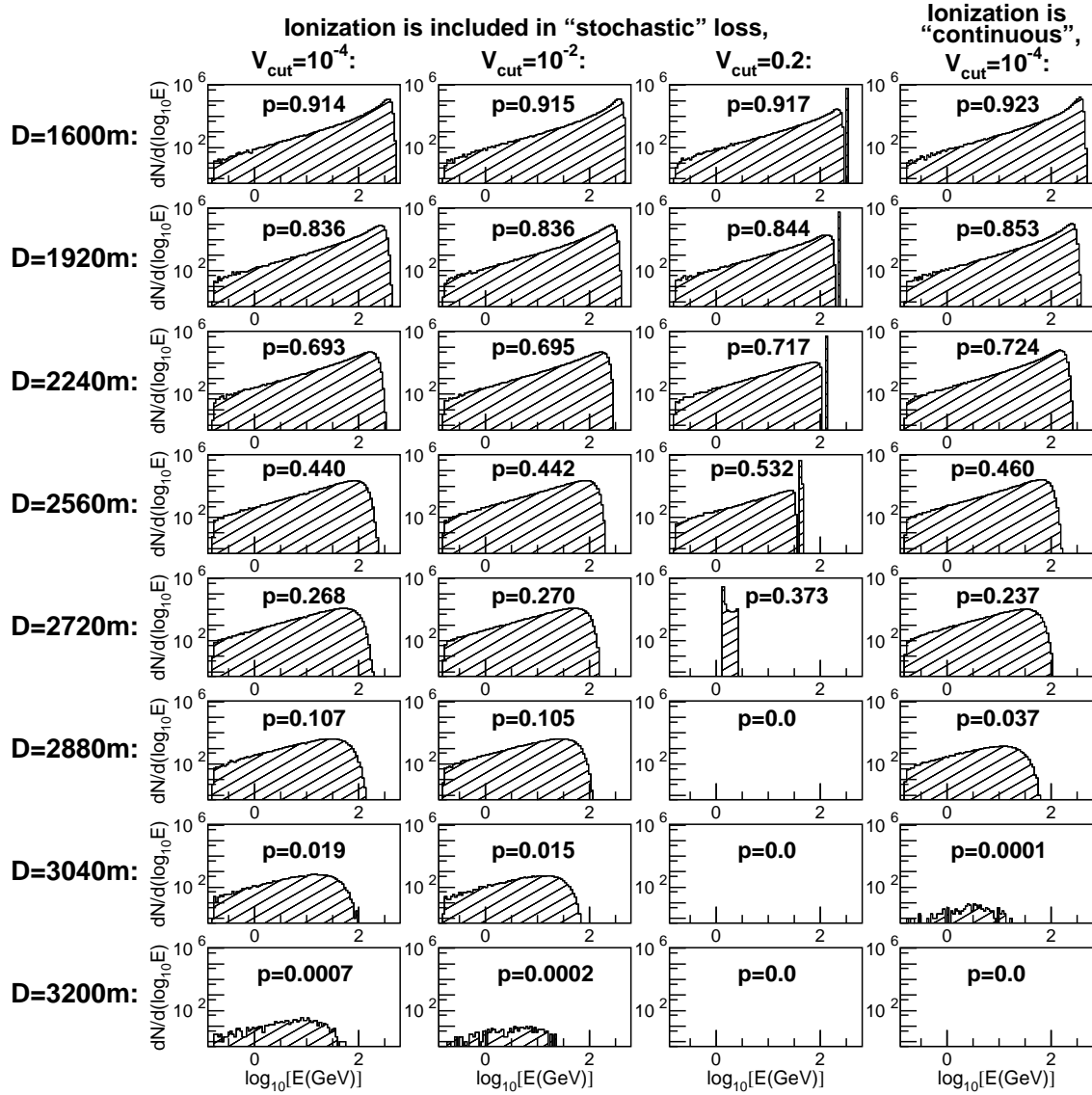


FIG. 7. Muon spectra resulting from 10^6 muons with initial energy $E_s = 1$ TeV as simulated with four models for different slant depths D in pure water. The first three columns represent spectra obtained with ionization included in SEL for $v_{cut} = 10^{-4}$ (1st column), 10^{-2} (2nd column), and 0.2 (3rd column). 4th column contains spectra obtained for entirely “continuous” ionization and $v_{cut} = 10^{-4}$. On each plot value of survival probability p is indicated without statistical error which does not exceed 1%.

It was shown above *what is result* of simulations with different models of ionization and values of v_{cut} . It was a special point of interest for us to track *how and why* does it influence upon behavior of survival probability. Fig. 7 shows how muon spectrum resulting from mono-energetic muon beam with initial energy $E_s = 1$ TeV transforms when its propagation being simulated through pure water down to the slant depth of 3.2 km. Results for four settings of parameters are presented by four columns of plots. The first three columns represent spectra obtained with ionization included in SEL for $v_{cut} = 10^{-4}$, 10^{-2} and 0.2. 4th column contains spectra simulated with entirely “continuous” ionization and $v_{cut} = 10^{-4}$. The spectra grouped into the first column represent the most accurate tuning both for v_{cut} and ionization model. The first three columns demonstrate that compactness of spectra at the same slant depth is the higher the more value of v_{cut} is. Put your attention to the right edge of spectra which shifts toward low energies when v_{cut} increases (it is the most noticeably for $v_{cut} = 0.2$). The reason is that at any slant depth energy of the most energetic muons in simulated beam is determined by CEL. These muons due to statistical fluctuations did not undergo interactions with $v \geq v_{cut}$ and, consequently, lost energy only by CEL which grows when v_{cut} increases. That is why the maximum energy in simulated muon beam is lower for large values of v_{cut} . Fraction of muons which did not undergo an “catastrophic” act with $v \geq v_{cut}$ till given slant depth grows with increase of v_{cut} because free path between two sequential interactions with $v \geq v_{cut}$ grows approximately as $\bar{L} \propto v_{cut}$. It leads, in particular, to

distinctly visible separated picks in spectra for $v_{cut} = 0.2$ consisted just of muons which lost energy only by CEL. Also some deficit of low energy muons appears if one sets v_{cut} to a large value. In this case left edge of spectrum is provided only with muons which interacted with large fraction of energy lost while for smaller v_{cut} an additional fraction of muons comes here. As a result simulated spectrum of initial mono-energetic muons at given slant depth is more narrow if v_{cut} is large and, on the contrary, more wide if v_{cut} is small.

Now it is easy to understand how value of v_{cut} influences on simulated survival probabilities. When simulated muon beam goes through a medium losing energy both in CEL and SEL processes, its spectrum is constantly shifting to the left (energy decreases). For $v_{cut} = 10^{-4}$ the left part of spectrum reaches $E = 0$ at a smaller slant depth comparing with larger v_{cut} and survival probability starts to decrease. At the same slant depth survival probability for $v_{cut} = 10^{-2}$ and $v_{cut} = 0.2$ is still equal to 1. Thus, for the first part of path the survival probability is always larger for large v_{cut} . At some slant depth (which is equal to ~ 2.8 km in the given case) compactness of spectra simulated with large v_{cut} starts to play an opposite role. Due to more powerful CEL muons stop faster comparing with accurate simulation. So at the final part of the beam path simulated survival probability for large v_{cut} decreases faster comparing with accurate simulation and, for instance, for $v_{cut} = 0.2$ the rest of muon beam which reaches the slant depth $D = 2.72$ km (37% of initial number of muons) completely vanishes within the next 30 m of path, while some fraction of muons simulated with $v_{cut} = 10^{-4}$ (0.07%) escapes down to the slant depth of $D = 3.2$ km. Qualitatively the same effect leads to the same consequences if one treats ionization as completely “continuous” process. Again, spectra becomes more narrow since fluctuations in ionization do not work and, as a consequence, survival probability becomes significantly higher comparing with simulation with accurate treatment of ionization at the beginning of muon beam path and falls down essentially faster at the final part of path.

Results presented above showed the significant influence which both model of ionization and value of v_{cut} have over survival probability for mono-energetic muon beam. But for practical purposes the more important is *how these factors do work for real atmospheric muons with a power spectrum?* In Fig. 8 we present intensity of vertical atmospheric muon flux I at different depths of pure water D from 1 km to 20 km vs. v_{cut} as simulated with muons sampled according to sea level spectrum Eq. (4.1). Simulation continued until 10^4 muons reached given depth. Curves for two models of ionization are shown for each depth along with results for $k_\sigma = 1.00 \pm 0.01$ at $v_{cut} = 10^{-4}$, parameterization for $\sigma_{\gamma N}$ from Ref. [36] at $v_{cut} = 10^{-4}$, sea level muon spectrum Eq. (4.2) at $v_{cut} = 10^{-4}$ and all energy losses treated entirely as CEL (for depths $D \leq 5$ km only). General conclusions for case with atmospheric muons are qualitatively the same as observed for mono-energetic muon beams but quantitatively the influence of v_{cut} and model of ionization energy losses on the resulting muon flux at large depths is much weaker. One can conclude the following:

- (a) Except for case $D = 1$ km computed muon flux is strongly affected by accounting for fluctuations in energy losses: muon flux intensity simulated with non-stochastic model of energy loss is less comparing with stochastic model by 10 % at 3 km w.e. and by 20% at 5 km w.e.. At the depth of 20 km of pure water vertical muon flux computed with ignorance of fluctuations is only 10 % of simulated flux.
- (b) Like a case with mono-energetic beams 1%-uncertainty in muon cross sections plays the principal role for resulting error in simulated muon depth intensity. This error has a tendency to grow with depth from $\pm 2.5\%$ at depth of 1 km w.e. to $\sim \pm 15\%$ at 20 km w.e.. But a particular case of this uncertainty, namely difference between parameterizations for $\sigma_{\gamma N}$ from Refs. [35,36], does not lead to a significant difference in resulting intensity.
- (c) Difference between muon spectra Eq. (4.1) and Eq. (4.2) leads to uncertainty from -4% ($D = 1$ km) to 16% ($D = 20$ km).
- (d) Error which appears due to simplified, entirely “continuous” ionization lies, commonly, at the level of $2 \div 3\%$.
- (e) Dependence of simulated muon flux intensity upon v_{cut} is the most weak one comparing with other studied error sources. Function $I(v_{cut})$ is almost a constant at $v_{cut} \leq 0.05$ and changes in a range $\pm 1 \div 2\%$ which is very close to statistical error. Up to $v_{cut} = 0.1$ the contributed error is less than one which comes from $\pm 1\%$ -uncertainty with the muon cross sections. Also no statistically significant influence of v_{cut} upon the shape of differential atmospheric muon spectra was observed at all tested depths for $10^{-4} \leq v_{cut} \leq 0.2$ for both models of ionization energy loss.

Results reported in this Section are evidence of accuracy in parameterizations for muon cross sections and sea level spectrum to be the principal source of uncertainties when simulating atmospheric muon flux at depths where neutrino telescopes are located. It contributes uncertainty from 3% (at the depth $D = 1$ km in pure water) to 15% ($D = 20$ km) in resulting intensity of muon flux. Unfortunately, this level has at present to be considered as a limit for accuracy of muon propagation algorithms. Influence of model for ionization exceeds this limit only for mono-energetic muon beams with initial energies $E \leq 10$ TeV and only if level of observation is at very last stage of muon range where major fraction of initial muon energy has been lost. Actually, due to steep shape of atmospheric muon power

spectrum, an essential part of muons reaches detector location being just on the last part of path. Therefore effect remains noticeable also for real atmospheric muons but in this case uncertainty was found to be much less: 2–3%, which is in an excellent agreement with Refs. [12,24], while Ref. [25] predicts much more significant difference (up to 17%). We suppose this disagreement may result from the fact that “small transfer grouping” technique used in Ref. [25] treats muon cross sections to be constant between two interactions in contrast with the MUM algorithm. In Ref. [24] the same simplification was used but reported results were obtained by simulation with $v_{cut} = 10^{-3}$. With such small v_{cut} role of correct treatment for free path is not significant (see Sec. II and Fig. 1). Choice of value for v_{cut} is of even less importance and again, it is more critical if one investigates mono-energetic muon beam but for power spectrum alteration in v_{cut} within $v_{cut} \leq 0.05$ leads only to 1–2% differences in simulated muon flux intensities. Up to $v_{cut} = 0.1$ the error caused by rough account for fluctuations in energy losses remains less than one which comes from uncertainties with muon energy loss. This conclusion is in a good agreement with level of errors reported in Ref. [24]. Differences between muon flux intensities simulated for different models of ionization and values of v_{cut} , as obtained in given work and in Refs. [24,25], are presented in Fig. 9 and Fig. 10.

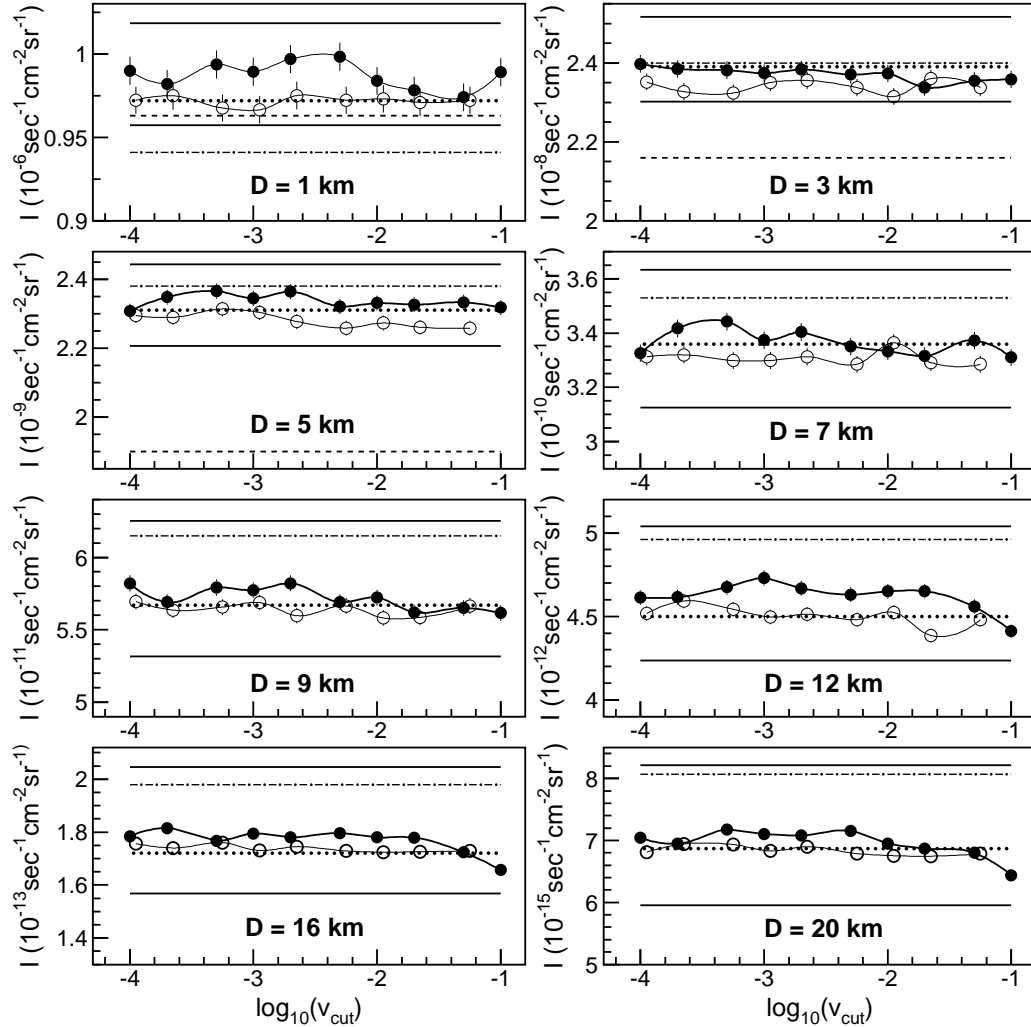


FIG. 8. Intensity of vertical atmospheric muon flux I at different depths D of pure water vs. v_{cut} as obtained by simulation with muons sampled according to sea level spectrum from Ref. [33] (Eq. (4.1)). Closed circles: ionization is included in SEL; open circles: ionization is completely “continuous”. Two horizontal solid lines on each plot show value for survival probability simulated with all muon cross sections multiplied by a factor $k_{\sigma} = 1.01$ (lower line) and $k_{\sigma} = 0.99$ (upper line) for $v_{cut} = 10^{-4}$. Dashed lines on plots for $D \leq 5$ km correspond to intensity which was calculated for all energy losses treated as “continuous”. Dash-dotted lines show intensity of vertical muon flux simulated with ionization included in SEL, $v_{cut} = 10^{-4}$ and muons sampled according to the Gaisser sea level spectrum (Ref. [34], Eq. (4.2)). Horizontal dotted lines correspond to $v_{cut} = 10^{-4}$ and cross section for absorption of a real photon at photo-nuclear interaction parameterized according to Ref. [36] instead of parameterization proposed in Ref. [35] which is basic in MUM.

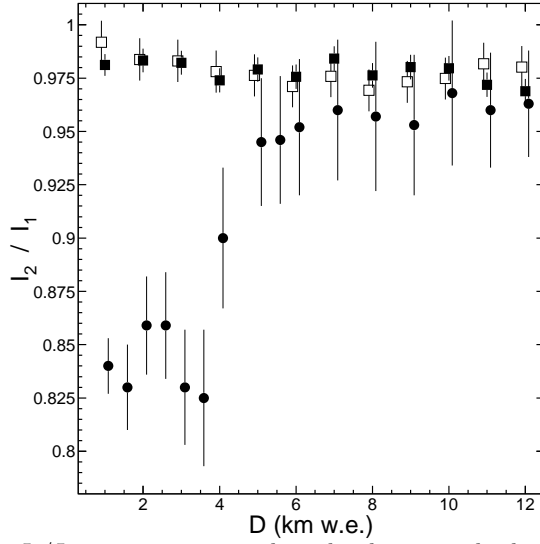


FIG. 9. Dependencies for relation I_2/I_1 vs. water equivalent depth in standard rock as computed in this work (closed squares), in Ref. [24] (open squares) and in Ref. [25] (closed circles). I_1 is depth intensity for vertical atmospheric muon flux simulated with ionization included in SEL, I_2 is one simulated with entirely “continuous” ionization. Data for this work are obtained for sea level atmospheric muon spectrum from Ref. [33] (Eq. (4.1)) and $v_{cut} = 10^{-3}$; data from Ref. [24] represent result of simulation for sea level spectrum from Ref. [34] (Eq. (4.2)) and $v_{cut} = 10^{-3}$; data from Ref. [25] were simulated with spectrum from Ref. [37] with “small transfer grouping” technique.

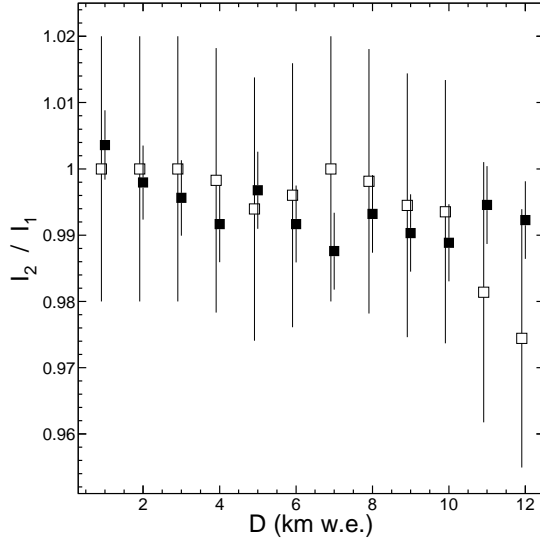


FIG. 10. Dependencies for relation I_2/I_1 vs. water equivalent depth in standard rock as computed in this work (closed squares) and in Ref. [24] (open squares). I_1 is depth intensity for vertical atmospheric muon flux simulated with entirely “continuous” ionization and $v_{cut} = 10^{-3}$, I_2 is one simulated with the same treatment of ionization and $v_{cut} = 10^{-2}$. Data for this work are obtained for sea level spectrum from Ref. [33] (Eq. (4.1)); data from Ref. [24] represent result of simulation for spectrum from Ref. [34] (Eq. (4.2)).

So when simulating muon fluxes at large depths with an “ideal MC muon propagation algorithm” it is reasonable to use $v_{cut} \approx 0.05 \div 0.1$ and entirely “continuous” model for ionization. Such setting of simulation parameters does not lead to the error which would be out of insuperable uncertainties with muon energy loss but allows to save the computation time essentially. Fig. 11 show dependence of computation time on v_{cut} and model for ionization, as was obtained with the MUM algorithm. Data for muon transportation codes PROPMMU (Ref. [22]) and MUSIC (Ref. [24]) are given on the figure, as well. We must emphasize that MUM in its presented version is 1D algorithm, in contrast both to PROPMMU and MUSIC. PROPMMU treats only Coulomb multiple scattering while in MUSIC the angle of the muon acquired in all radiative processes is also simulated which takes an additional computation time. We evaluate the factor by which computation time with MUM would increase in case of extension up to 3D-algorithm as ~ 2 .

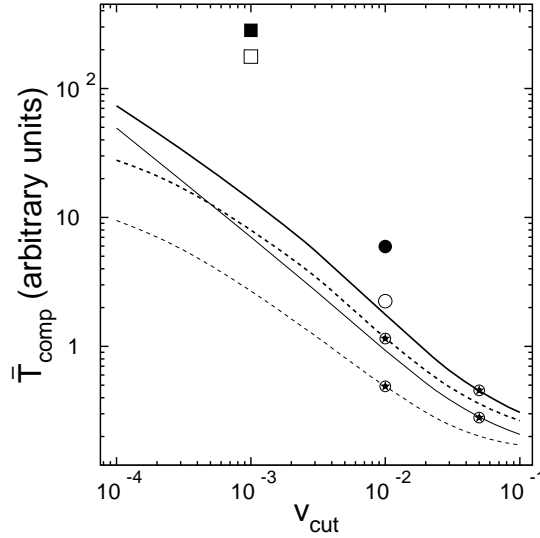


FIG. 11. Averaged computation time \bar{T}_{comp} which is necessary for muon propagation in pure water vs. v_{cut} , as obtained with the MUM code. Thick lines correspond to muon with initial energy $E_s = 9$ TeV transported down to $D = 10$ km. Thin lines are for $E_s = 1$ TeV and $D = 3$ km. Solid lines show results for ionization included in SEL, dashed ones correspond to entirely “continuous” ionization. Circled asterisks on curves correspond to conservatively evaluated upper boundary for v_{cut} below which the MUM algorithm inner accuracy has been proved to be high enough. This limit is equal to $v_{cut} = 0.05$ if ionization is included in SEL and to $v_{cut} = 0.01$ if ionization is entirely “continuous” (see Sec. III). Circles and squares show values for \bar{T}_{comp} , as obtained with muon propagation codes PROPUMU (version 2.01, 18/03/1993 with $v_{cut} = 10^{-2}$ which is unchangeable) and MUSIC (version for pure water with bremsstrahlung cross sections by Kehlner-Kokoulin-Petrukhin, 04/1999 with $v_{cut} = 10^{-2}$ which is unchangeable), correspondingly. Closed markers are for $E_s = 9$ TeV and $D = 10$ km, open ones are for $E_s = 1$ TeV and $D = 3$ km.

Accounting for data on real accuracy of current version of the MUM code (see Sec. III) which and data on computation time presented in Fig. 11 we conservatively consider $v_{cut} = 0.05$ and knock-on electron production included in SEL as an optimum setting for presented algorithm which allows to obtain the accurate results with relatively high speed. With such setting the proportion of computation time which is necessary to get the same statistics with MUM, PROPUMU and MUSIC is approximately 1 : 10 : 600. Of course, for some methodical purposes it may be necessary to choose more fine v_{cut} , e.g. if one wants to exclude an additional error when comparing results of simulations for different models of atmospheric muon sea level spectrum with each other or investigating survival probabilities which are much more sensitive to value of v_{cut} than simulated spectrum of atmospheric muons at large depths.

We did not investigate specially the influence of simulation parameters on the results for the muon flux originated from neutrino but simple argumentation may be applied for this case. In contrast with atmospheric muons whose source is far away of underwater, under-ice or underground detector and whose flux may only decrease when passing from the sea level down to detector depth, the source for muons which are produced in νN interactions is uniformly distributed over water and/or rock both out- and inside the array. Intensity of the muon flux I_μ^{ac} which accompanies the neutrino flux in a medium is proportional to the muon range, and, consequently, $I_\mu^{ac} \propto (dE/dx)_{total}^{-1}$ while simulated flux of atmospheric muons at large depths depends more sharply upon muon energy loss as was shown in this Section. Thus, one may conclude that the setting of parameters described above fits even better for propagation of muons originated from neutrino.

It is impossible to foresee all particular cases and give some strict conformity between setting of parameters at muon MC propagation code and problem to be solved. But we tried to present in this Section the whole set of data which are necessary to chose the optimum set in each concrete case.

V. SELECTED RESULTS AND COMPARISON WITH OTHER ALGORITHMS

In this Section we present selected data on survival probabilities and atmospheric muon spectra deep underwater as simulated with MUM. To obtain atmospheric muon spectra we set $v_{cut} = 0.05$. As was shown in Sec. III and Sec. IV it does not distort results comparing to simulation with smaller values of v_{cut} . To compute survival probabilities more delicate tuning was applied: $v_{cut} = 10^{-3}$. In both cases ionization was included in SEL. We compare our data with ones obtained with the PROPUMU and MUSIC algorithms. Data simulated with PROPUMU [version 2.01,

18/03/1993] ($v_{cut} = 10^{-2}$) and PROPMU [version 2.1, 01/2000] (both with $v_{cut} = 10^{-3}$ and $v_{cut} = 10^{-2}$) are very close to each other, in all figures of this Section results from PROPMU [version 2.01, 18/03/1993] are presented. We used [version for pure water with bremsstrahlung cross sections by Kelner-Kokoulin-Petrushin, 04/1999] with $v_{cut} = 10^{-3}$ for MUSIC. When comparing results on atmospheric muons at large depths obtained for pure and sea water the data are recalculated to each other using value $\rho = 1.027 \text{ g cm}^{-3}$ as a sea water density (Ref. [38,39]). The difference between pure and sea water is negligible small for the muon propagation if one works in water equivalent units which was tested by us up to slant depth $D = 10 \text{ km}$ w.e. (see also Ref. [13]).

Fig. 12 shows survival probabilities vs. slant depth D in pure water as simulated for a set of initial muon beam energies from $E_s = 500 \text{ GeV}$ to $E_s = 30 \text{ PeV}$. Survival probabilities obtained with MUM coincide within statistical errors with ones computed with MUSIC. PROPMU gives remarkably different values which are higher comparing to MUM and MUSIC output at muon energies $E_s \leq 30 \text{ TeV}$ and become less at $E_s > 30 \text{ TeV}$.

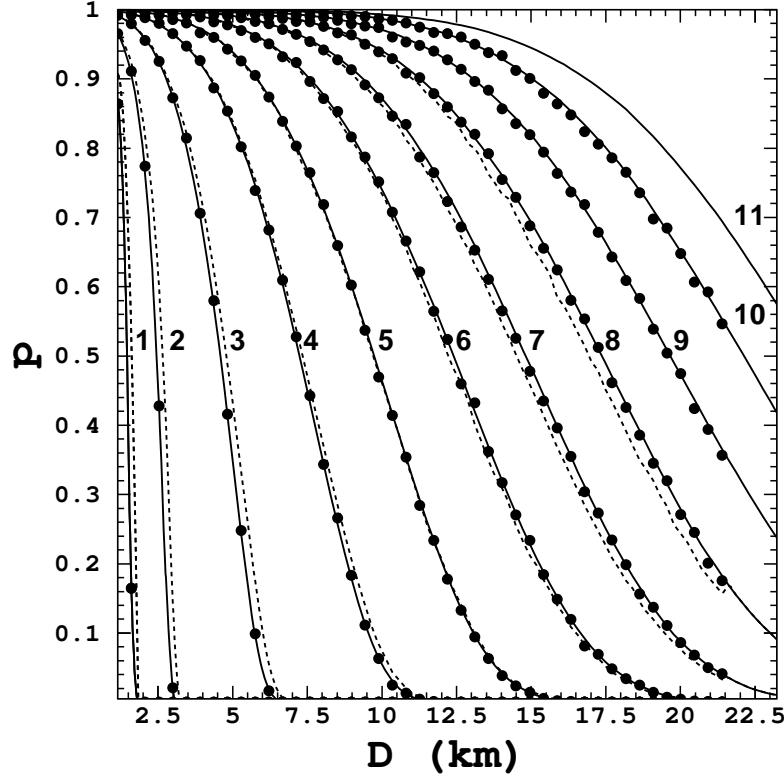


FIG. 12. Survival probabilities vs. slant depth D in pure water as computed with MUM (solid lines), MUSIC (circles), and PROPMU (dashed lines). Figures near curves indicate initial energies of muon beams which were as follows: 500 GeV (1), 1 TeV (2), 3 TeV (3), 10 TeV (4), 30 TeV (5), 100 TeV (6), 300 TeV (7), 1 PeV (8), 3 PeV (9), 10 PeV (10), 30 PeV (11). At simulations of data presented on the plot muons are treated as stopped as soon as their energy decreases down to 10 GeV.

Fig. 13 gives more detailed data on survival probabilities for three particular cases. It presents muon spectra resulted from mono-energetic muon beams with initial energies $E_s = 1 \text{ TeV}$ (Fig. 13(a)), $E_s = 9 \text{ TeV}$ (Fig. 13(b)) and $E_s = 1 \text{ PeV}$ (Fig. 13(c)) after propagation of distances 3 km, 10 km and 40 km in pure water, correspondingly. The distances were chosen so that survival probabilities would be much less than 1 in which case differences become more noticeable (see Sec. IV). A good agreement is observed between MUM and MUSIC data, while data obtained with PROPMU indicate essential differences which are of the same signs as in Fig. 12.

In Fig. 14 differential spectra for vertical atmospheric muons at different depths in pure water are presented as simulated with MUM, PROPMU and MUSIC. Muons at the surface were sampled according to spectrum Eq. (4.1). Also parameterizations for deep underwater muon spectra as proposed by A. Okada in Ref. [40] and by S. Klimushin *et al.* in Ref. [33] (from here on will call them “the Okada parameterization” and “the KBS parameterization”, correspondingly) are shown. The KBS parameterization can adopt different models for sea level atmospheric muon spectrum. For data presented in Fig. 14 we used spectrum Eq. (4.1) which is basic one for the KBS parameterization. MUM gives almost the same results as MUSIC which could be expected because survival probabilities for muons in pure water are the same when simulating with MUSIC and MUM, as was shown above. Simulation with PROPMU

produces the muon spectra which (a) are significantly higher (31%, 30%, 27% and 17% in terms of integral muon flux at the depths $D = 1$ km, 3 km, 6 km and 10 km, correspondingly) and (b) are expanded to the low energies. It is in good qualitative agreement with results on survival probabilities presented in Fig. 12 and Fig. 13. The coincidence between spectra simulated with MUM and curves for the basic KBS parameterization results from the fact that in both cases the same sea level atmospheric muon spectrum was adopted and, besides muon transport with the MUM algorithm was applied to obtain the KBS parameterization. We would like to mark that survival probabilities which KBS parameterization is based on were computed with $v_{cut} = 10^{-3}$. An excellent agreement with direct simulation in which $v_{cut} = 0.05$ was set confirms the conclusion concerning insensitivity of results on simulated atmospheric muon spectra at large depths on value of v_{cut} up to at least $v_{cut} = 0.05$ (see Sec. IV). The Okada parameterization is lower than KBS, MUM and MUSIC results (up to 18% in terms of integral muon flux at $D = 1$ km) at relatively shallow depths and becomes higher at $D \geq 5$ km because it is based on rather hard sea level atmospheric muon spectrum with index $\gamma = 2.57$ (Ref. [41]) which leads to a deficit for low energy muons comparing to the basic KBS parameterization.

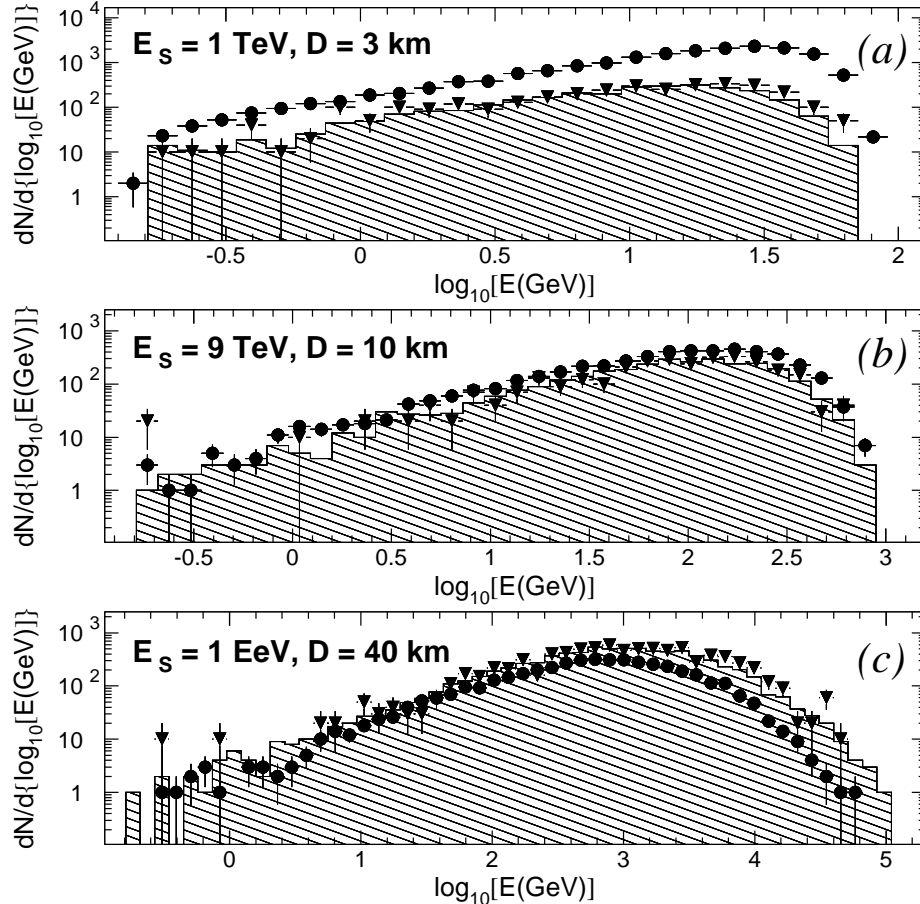


FIG. 13. Muon spectra resulting from mono-energetic muon beams with initial energies $E_s = 1$ TeV (a), $E_s = 9$ TeV (b) and $E_s = 1$ EeV (c) after propagation down to depths $D = 3$ km, 10 km and 40 km of pure water, correspondingly, as simulated with MUM (histograms), PROPMU (circles), and MUSIC (triangles). Corresponding values for survival probabilities p (fraction of muons survived after propagation) are equal to: $p(1 \text{ TeV}, 3 \text{ km}) = 0.029$ (MUM), 0.033 (MUSIC), 0.19 (PROPMU); $p(9 \text{ TeV}, 10 \text{ km}) = 0.030$ (MUM), 0.031 (MUSIC), 0.048 (PROPMU); $p(1 \text{ PeV}, 40 \text{ km}) = 0.078$ (MUM), 0.084 (MUSIC), 0.044 (PROPMU).

Fig. 15 presents results on integral flux of vertical atmospheric muons at large depths in pure water as (a) simulated with MUM, PROPMU and MUSIC for sea level spectrum Eq. (4.1); (b) parameterized by KBS (Ref. [33]) with sea level atmospheric muon spectra Eq. (4.1) (basic), from Ref. [34] (the Gaisser spectrum), from Ref. [42] (the MACRO spectrum) and A. Okada (Ref. [40]) with sea level spectrum from Ref. [41]; (c) measured by S. Higashi *et al.* (Ref. [38]), V. M. Fedorov *et al.* (Ref. [43]) and Yu. N. Vavilov *et al.* (Ref. [44]). Note that “experimental” points on the plot does not represent the pure experimental data because authors had to recalculate obtained counting rates to the vertical direction using a model for the muon angular spectrum underwater. MUM and MUSIC results coincide with each

other within $1\div 2\%$. Results from PROPMU algorithm exceed points from MUSIC and MUM by $\sim 30\%$ being higher than any of presented parameterizations.

We also compared the data on muon propagation through the standard rock obtained with MUM and MUSIC. Mean energy for vertically down-going atmospheric muons sampled with sea level spectrum from Ref. [34] was computed with MUM as $\bar{E} = 123\pm 2$ GeV, 256 ± 4 GeV and 387 ± 7 GeV at depths $D = 1$ km w.e., 3 km w.e. and 10 km w.e., respectively. The corresponding values simulated with the MUSIC code and reported in Ref. [24] are $\bar{E} = 125\pm 1$ GeV, 259 ± 3 GeV and 364 ± 4 GeV. So the maximum difference observed at the depth $D = 10$ km w.e. is of 6%.

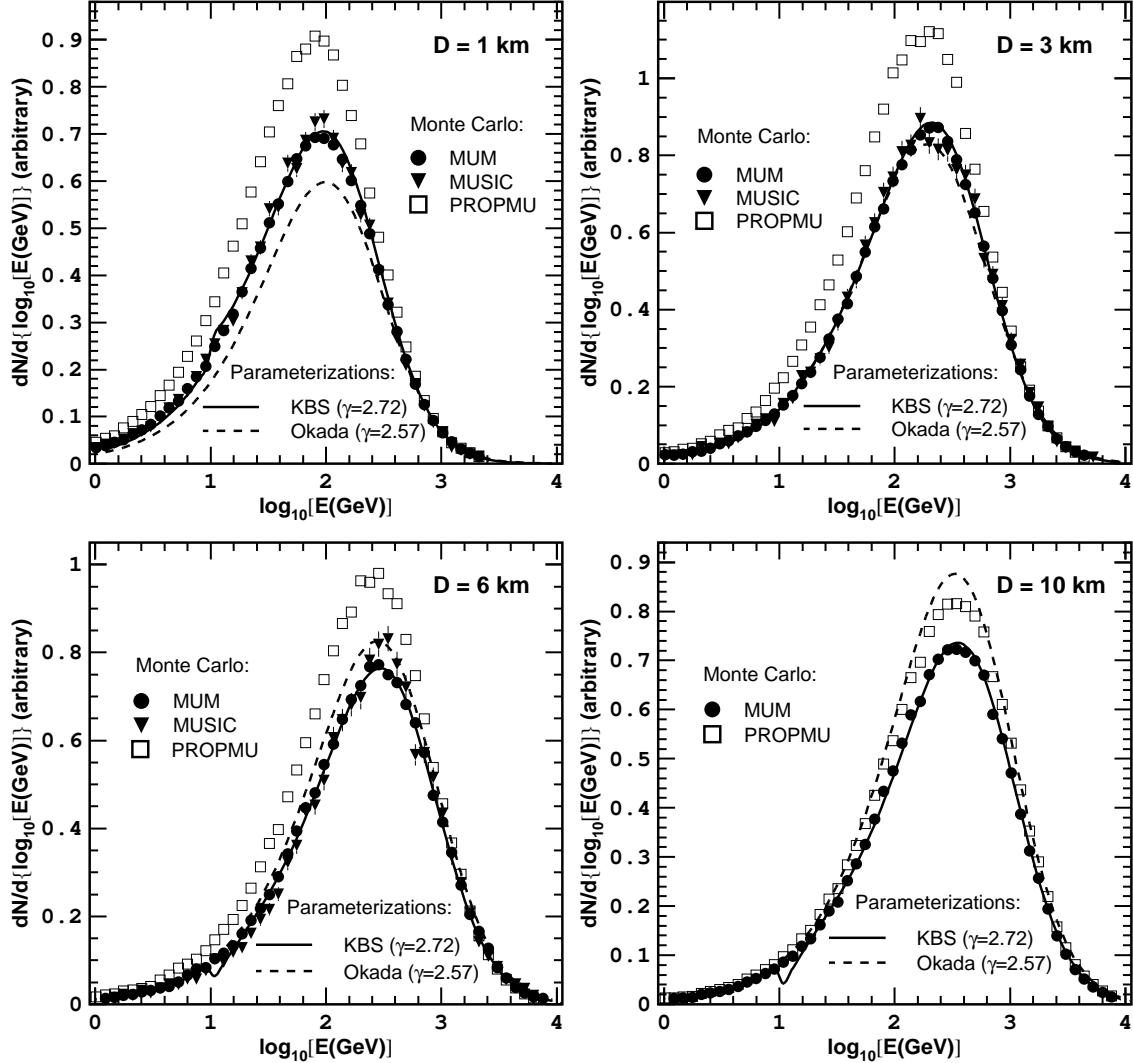


FIG. 14. Differential spectra of vertical atmospheric muons at four depths in the pure water as simulated with MUM, PROPMU and MUSIC (in all cases muon energies at the sea level were sampled according to spectrum Eq. (4.1)) and parameterized according to KBS with sea level spectrum Eq. (4.1) (Ref. [33]) and A. Okada (Ref. [40]).

Thus, results on survival probabilities and atmospheric muon spectra at large depths as simulated with MUM are practically in a coincidence with ones obtained with MUSIC and are not also in contradiction with any experimental and theoretical results presented in this section. The PROPMU algorithm shows noticeable differences with MUM which are in good qualitative agreement to each other: higher survival probabilities lead to higher muon fluxes deep underwater. It is difficult to clarify the source of observed discrepancies without detailed comparison for all steps of the algorithms but we believe that they can not be explained only by a difference in models for muon energy loss as it is used in MUM (see Appendix A) and PROPMU (Refs. [19,22]) which does not exceed 2% at $E \leq 10$ TeV (in terms of stopping power) being besides of both signs.

More data obtained with the MUM algorithm can be found in Ref. [33].

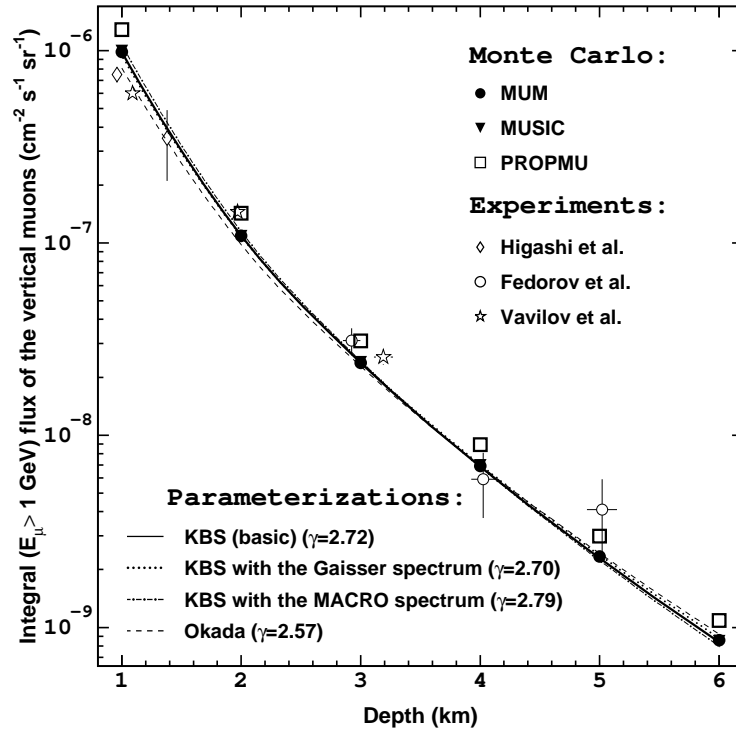


FIG. 15. Results for integral flux of vertical atmospheric muons vs. depth in pure water as (1) simulated with MUM, PROPMU and MUSIC with sea level spectrum Eq. (4.1); (2) parameterized by KBS (Ref. [33]) with sea level atmospheric muon spectra Eq. (4.1) (basic), from Ref. [34] (the Gaisser spectrum), from Ref. [42] (the MACRO spectrum) and A. Okada (Ref. [40]) with sea level spectrum from Ref. [41]; (3) measured by S. Higashi *et al.* (Ref. [38]), V. M. Fedorov *et al.* (Ref. [43]) and Yu. N. Vavilov *et al.* (Ref. [44]).

VI. CONCLUSIONS

We have presented the muon propagation Monte Carlo FORTRAN code MUM (MUons+Medium) and have given selected results obtained with the code for muon spectra at large depths and survival probabilities in comparison with results obtained with other muon transportation algorithms. It was shown that for majority of applications it is quite enough to account only for fluctuations in the radiative energy loss with fractions of energy lost as large as $v \geq v_{cut} = 0.05 \div 0.1$ while ionization energy loss may be entirely accounted by stopping power formula, as well as radiative energy loss with fractions of energy lost $v < v_{cut} = 0.05 \div 0.1$. This gives an essential advantage in terms of computation time comparing to commonly used $v_{cut} = 10^{-3} \div 10^{-2}$ without loss of accuracy when simulating both propagation of atmospheric muons and muons which are born in νN interactions. However in practice it makes particular demands to accuracy of MC algorithm. Some customary simplifications (e.g. Eq (2.4)) which work perfectly when $v_{cut} = 10^{-3} \div 10^{-2}$ become sources of significant errors when v_{cut} increases. The sign and value of these errors depend also on whether fluctuations in ionization are accounted or not. So for presented version of the MUM algorithm the optimum set of simulation parameters was conservatively evaluated by us (accounting results on inner accuracy test and dependence of computation time on v_{cut}) to be $v_{cut} = 0.05$ and knock-electron production included in SEL.

Our point of view on advantages of MUM is as follows. It is flexible enough and provides with eventuality to tune parameters of simulation to an optimum for each concrete case to get desirable equilibrium between computation time and accuracy. Medium composition and parameterizations for muon cross sections are easily changeable. Inner accuracy of the code was conservatively evaluated to be 2×10^{-3} or better. Besides, MUM provides with the special routine which allows to test inner accuracy for each given set of simulation parameters and take it into account when evaluating significance of results. The main disadvantage is that MUM in its reported version does not still treat the three dimensions like, e.g. PROPMU and MUSIC codes. So it can not be used to obtain lateral and angular deviations of muons at propagation through matter. Also other important features are still missed in MUM - for instance, treatment of composed medium as it is possible, e.g. in the latest version of the MUSIC code (Ref. [45]). But we consider the current version of MUM as a basis for further development and plan to complement it, step by step, by all necessary features.

The MUM code is available on request to sokalski@pcbai10.inr.ruhep.ru.

ACKNOWLEDGMENTS

We would like to express our gratitude to I. Belolaptikov for useful discussions which allowed to improve the MUM algorithm essentially. We are grateful to A. Butkevich, R. Kokoulin, V. Kudryavzev, P. Lipari, W. Lohmann, V. Naumov, O. Streicher and Ch. Wiebusch who read the paper at the draft study and gave their comments which mostly were taken into account both in the final version of the article and in the algorithm itself. We thank an anonymous referee whose constructive and benevolent critique stimulated us for essential improvements in the article text. One of us (I.S.) was benefited a lot by attention and support of L. Bezrukov and Ch. Spiering.

APPENDIX A: PARAMETERIZATIONS FOR MUON CROSS SECTIONS USED IN THE MUM ALGORITHM

We use the following designations in this section: $\alpha = 7.297353 \times 10^{-3}$ – fine structure constant; $r_e = 2.817941 \times 10^{-13}$ cm – classical radii of electron; $m_\mu = 0.1056593$ GeV and $m_e = 0.5110034$ MeV – muon and electron masses, correspondingly; $N_A = 6.022 \times 10^{23}$ – the Avogadro number; Z and A – electric charge and atomic weight, correspondingly; $e = 2.718282$; $\pi = 3.141593$. Other notations are explained in comments to formulas when necessary.

1. Bremsstrahlung

We use differential cross section for bremsstrahlung as parameterized by Yu. M. Andreev, L. B. Bezrukov and E. V. Bugaev in Ref. [46] as a basic parameterization:

$$\begin{aligned} \frac{d\sigma^b}{dv}(E, v) &= \alpha \left(2r_e Z \frac{m_e}{m_\mu} \right)^2 \frac{1}{v} \left[(2 - 2v + v^2) \Psi_1(q_{\min}, Z) - \frac{2}{3} (1 - v) \Psi_2(q_{\min}, Z) \right], \\ \Psi_{1,2}(q_{\min}, Z) &= \Psi_{1,2}^0(q_{\min}, Z) - \Delta_{1,2}(q_{\min}, Z), \\ \Psi_1^0(q_{\min}, Z) &= \frac{1}{2} \left(1 + \ln \frac{m_\mu^2 a_1^2}{1 + x_1^2} \right) - x_1 \arctan \frac{1}{x_1} + \frac{1}{Z} \left[\frac{1}{2} \left(1 + \ln \frac{m_\mu^2 a_2^2}{1 + x_2^2} \right) - x_2 \arctan \frac{1}{x_2} \right], \\ \Psi_2^0(q_{\min}, Z) &= \frac{1}{2} \left(\frac{2}{3} + \ln \frac{m_\mu^2 a_1^2}{1 + x_1^2} \right) + 2x_1^2 \left(1 - x_1 \arctan \frac{1}{x_1} + \frac{3}{4} \ln \frac{x_1^2}{1 + x_1^2} \right) \\ &\quad + \frac{1}{Z} \left[\frac{1}{2} \left(\frac{2}{3} + \ln \frac{m_\mu^2 a_2^2}{1 + x_2^2} \right) + 2x_2^2 \left(1 - x_2 \arctan \frac{1}{x_2} + \frac{3}{4} \ln \frac{x_2^2}{1 + x_2^2} \right) \right], \\ \Delta_1(q_{\min}, Z \neq 1) &= \ln \frac{m_\mu}{q_c} + \frac{\zeta}{2} \ln \frac{\zeta + 1}{\zeta - 1}, \\ \Delta_2(q_{\min}, Z \neq 1) &= \ln \frac{m_\mu}{q_c} + \frac{\zeta}{4} (3 - \zeta^2) \ln \frac{\zeta + 1}{\zeta - 1} + \frac{2m_\mu^2}{q_c^2}, \\ \Delta_{1,2}(q_{\min}, Z = 1) &= 0, \end{aligned}$$

$$q_{\min} = \frac{m_\mu^2 v}{2E(1 - v)}, \quad x_i = a_i q_{\min},$$

$$a_1 = \frac{111.7}{Z^{1/3} m_e}, \quad a_2 = \frac{724.2}{Z^{2/3} m_e}, \quad \zeta = \sqrt{1 + \frac{4m_\mu^2}{q_c^2}}, \quad q_c = \frac{1.9m_\mu}{Z^{1/3}}.$$

Integration limits for bremsstrahlung in Eqs. (2.1), (2.3), (2.6) and (3.3) are

$$v_{min}^b = 0, \quad v_{max}^b = 1 - \frac{3}{4}\sqrt{e}(m_\mu/E)Z^{1/3}.$$

Note that this parameterization does not account for contribution from e -diagrams for bremsstrahlung when γ -quantum is emitted by atomic electrons which are knocked on by recoil (Ref. [47]). Corresponding corrections are done in parameterizations for knock-on electron production (see Appendix A 4) according to Ref. [48]. Optionally, differential cross section for muon bremsstrahlung can be also treated in MUM according to parameterization given by S. R. Kelner, R. P. Kokoulin, and A. A. Petrukhin (Ref. [47,48]).

2. Photo-nuclear interaction

We use parameterization for the photo-nuclear interaction of muon proposed by L. B. Bezrukov and E. V. Bugaev (Ref. [35]):

$$\begin{aligned} \frac{d\sigma^n}{dv} = & \frac{\alpha}{8\pi} A\sigma_{\gamma N} v \left\{ H(v) \ln \left(1 + \frac{m_2^2}{t} \right) - \frac{2m_\mu^2}{t} \left[1 - \frac{0.25m_2^2}{t} \ln \left(1 + \frac{t}{m_2^2} \right) \right] \right. \\ & \left. + G(z) \left[H(v) \left(\ln \left(1 + \frac{m_1^2}{t} \right) - \frac{m_1^2}{m_1^2 + t} \right) - \frac{2m_\mu^2}{t} \left(1 - \frac{0.25m_1^2}{m_1^2 + t} \right) \right] \right\}, \end{aligned}$$

$$H(v) = 1 - \frac{2}{v} + \frac{2}{v^2},$$

$$\begin{aligned} G(z) &= \frac{9}{z} \left[\frac{1}{2} + \frac{(1+z)e^{-z} - 1}{z^2} \right] \quad (Z \neq 1), \\ G(z) &= 3 \quad (Z = 1), \end{aligned}$$

$$z = 0.00282A^{1/3}\sigma_{\gamma N}, \quad t = \frac{m_\mu^2 v^2}{1-v}, \quad m_1^2 = 0.54 \text{ GeV}^2, \quad m_2^2 = 1.80 \text{ GeV}^2.$$

Total cross section for absorption of a real photon of energy $\nu = s/2m_N = vE$ by a nucleon, $\sigma_{\gamma N}$, can be calculated in MUM optionally according to either parameterization from Ref [35] (basic):

$$\sigma_{\gamma N} = [114.3 + 1.647 \ln^2(0.0213 \nu)] \mu b,$$

or by the ZEUS parameterization (Ref. [36]):

$$\sigma_{\gamma N} = (63.5 s^{0.097} + 145 s^{-0.5}) \mu b,$$

where s and ν are expressed in GeV^2 and GeV , correspondingly.

Parameterization (Ref. [35]) is valid for $\nu > 1 \text{ GeV}$ so we use values $v_{min}^n = 0.8/E(\text{GeV})$ and $v_{max}^n = 1$ as integration limits in Eqs. (2.1), (2.3), (2.6) and (3.3). Note that results of integration were tested to be almost insensitive to the lower limit in a wide range $0.2/E(\text{GeV}) \leq v_{min}^n \leq 1.5/E(\text{GeV})$.

3. Direct electron-positron pair production

Cross section for direct e^+e^- -pair production is used in MUM as parameterized by R. P. Kokoulin and A. A. Petrukhin (Refs. [48,49]):

$$\frac{d\sigma^p}{dv}(E, v) = \alpha^2 \frac{2}{3\pi} r_e^2 Z(Z + \zeta(Z)) \frac{1-v}{v} \int_{\rho} \left[\Phi_e + (m_e/m_\mu)^2 \Phi_\mu \right] d\rho,$$

$$\Phi_e = \left\{ \left[(2 + \rho^2)(1 + \beta) + \xi(3 + \rho^2) \right] \ln \left(1 + \frac{1}{\xi} \right) + \frac{1 - \rho^2 - \beta}{1 + \xi} - (3 + \rho^2) \right\} L_e,$$

$$\Phi_\mu = \left\{ \left[(1 + \rho^2) \left(1 + \frac{3}{2}\beta \right) - \frac{1}{\xi} (1 - \rho^2) (1 + 2\beta) \right] \ln(1 + \xi) + \frac{\xi (1 - \rho^2 - \beta)}{1 + \xi} + (1 - \rho^2) (1 + 2\beta) \right\} L_\mu,$$

$$L_e = \ln \left[\frac{R Z^{-1/3} \sqrt{(1 + \xi) (1 + Y_e)}}{1 + \frac{2m_e \sqrt{e} R Z^{-1/3} (1 + \xi) (1 + Y_e)}{E v (1 - \rho^2)}} \right] - \frac{1}{2} \ln \left[1 + \left(\frac{3}{2} \frac{m_e}{m_\mu} Z^{1/3} \right)^2 (1 + \xi) (1 + Y_e) \right],$$

$$L_\mu = \ln \left[\frac{\frac{2}{3} \frac{m_\mu}{m_e} R Z^{-2/3}}{1 + \frac{2m_e \sqrt{e} R Z^{-1/3} (1 + \xi) (1 + Y_e)}{E v (1 - \rho^2)}} \right],$$

$$Y_e = \frac{5 - \rho^2 + 4\beta (1 + \rho^2)}{2 (1 + 3\beta) \ln(3 + 1/\xi) - \rho^2 - 2\beta (2 - \rho^2)},$$

$$Y_\mu = \frac{4 + \rho^2 + 3\beta (1 + \rho^2)}{(1 + \rho^2) \left(\frac{3}{2} + 2\beta \right) \ln(3 + \xi) + 1 - \frac{3}{2} \rho^2},$$

$$\beta = \frac{v^2}{2(1 - v)}, \quad \xi = \left(\frac{m_\mu v}{2m_e} \right)^2 \frac{(1 - \rho^2)}{(1 - v)}.$$

Here $\rho = (\epsilon^+ - \epsilon^-)/(\epsilon^+ + \epsilon^-)$ is the asymmetry coefficient of the energy distribution of e^+e^- -pair, ϵ^+ and ϵ^- are positron and electron energies, correspondingly. Limits for integration over ρ are determined by:

$$0 \leq |\rho| \leq \left(1 - \frac{6m_\mu^2}{E^2(1 - v)} \right) \sqrt{1 - \frac{4m_e}{Ev}}.$$

R is a parameter determined by the value of radiation logarithm ($R = 183$ for Thomas-Fermi model and slightly depends upon Z for Hartrey-Fock model). Its values are taken from Ref. [50], where R has been calculated for different atoms according to Hartrey-Fock model. $\zeta(Z) \approx 1$ takes into account the pair production in collisions with electrons. Values from $\zeta(Z)$ are computed according to Refs. [48,51]. Integration limits for $j = p$ in Eqs. (2.1), (2.3), (2.6) and (3.3) are

$$v_{min}^p = \frac{4m_e}{E}, \quad v_{max}^p = 1 - \frac{3}{4} \sqrt{e} (m_\mu/E) Z^{1/3}.$$

4. Knock-on electron production

Cross section for knock-on electron production is parameterized in the MUM algorithm as follows:

$$\frac{d\sigma^e}{dv}(E, v) = 2\pi r_e^2 Z \frac{m_e}{E} \left(\frac{1}{v^2} - \frac{1}{v} \frac{E}{v_{max}^e} + \frac{1}{2} \right) (1 + \Delta_{e\gamma}(E, v)),$$

$$v_{max}^e = \frac{2m_e E}{m_\mu^2 + 2m_e E}.$$

$\Delta_{e\gamma}(E, v)$ represents the correction which takes into account e -diagrams for bremsstrahlung (Refs. [47,48]) resulting in additional recoil electrons:

$$\Delta_{e\gamma}(E, v) = \frac{\alpha}{2\pi} \ln \left(1 + \frac{2vE}{m_e} \right) \left[\ln \left(\frac{4E^2(1 - v)}{m_\mu^2} \right) - \ln \left(1 + \frac{2vE}{m_e} \right) \right],$$

value of v_{max}^e is used also as upper integration limit in Eqs. (2.3) and (2.6) for $j = e$.

5. Ionization

Following Refs. [47,48] we treat in the MUM code e -diagrams for bremsstrahlung as a part of ionization process. Therefore we have to use a bit modified formula for ionization:

$$\left[\frac{dE}{dx}(E) \right]_{ion} = \frac{K}{\beta^2} \frac{Z}{A} \rho \left[\ln \left(\frac{2m_e p^2 E_{\max}}{m_\mu^2 \bar{I}^2} \right) + \frac{E_{\max}^2}{4E^2} - 2\beta^2 - \delta \right] + \frac{N_A}{A_{eff}} \rho E \sum_{i=1}^n \left[k_i \int_0^{v_{max}^e} \Delta_{e\gamma}(E, v) v dv \right].$$

Here $K = 0.1535 \text{ MeV g}^{-1} \text{ cm}^2$, p is the muon momentum, $\beta = p/E$ is the muon velocity, ρ is the material density, \bar{I} is the mean ionization potential,

$$E_{\max} = (2m_e p^2)/(m_\mu^2 + m_e^2 + 2m_e E)$$

is the maximum energy transferable to an electron, δ is the density-effect correction which is treated according to Ref. [52]:

$$\delta = \theta(X - X_0) [4.6052X + a\theta(X_1 - X)(X_1 - X)^m + C],$$

where θ is the step function ($\theta(x) = 0$ at $x \leq 0$ and $\theta(x) = 1$ at $x > 0$), $X = \log_{10}(p/m_\mu)$. The values X_0 , X_1 , a , m and C depend on the material and can be found in Refs. [19,52] along with values for \bar{I} , ρ and Z/A . The first term represents Bethe-Bloch formula with corrections for density effect, the second one accounts bremsstrahlung e -diagrams. Expressions for $\Delta_{e\gamma}(E, v)$ and v_{max}^e are given in Appendix A 4, meaning of values A_{eff} and k_i is explained in Sec. II.

APPENDIX B: FREE PATH BETWEEN TWO MUON INTERACTIONS

For the proof of the set of equation Eqs. (2.2) it is convenient to introduce the kinetic equation for a propagation of a mono-energetic muon beam through a medium. With the notations used in textbooks this equation has the following view:

$$\begin{cases} \partial n(E, t)/\partial t - \partial[\beta(E)n(E, t)]/\partial E + n(E, t)/\lambda(E) = 0 \\ n(E, 0) = n_0 \delta(E - E_0) \end{cases} \quad (\text{B1})$$

Here, $n(E, t)$ is the number of muons with energy E after propagation of distance t , $\beta(E)$ is the “continuous” energy loss per unit path, $\lambda(E)$ is the muon mean free path before interaction of SEL type. The solution of Eq. (B1) is:

$$n(E, t) = n_0 \delta(E - \epsilon(E_0, t)) \exp \left[- \int_E^{E_0} dE' / \left(\lambda(E') \beta(E') \right) \right], \quad (\text{B2})$$

where $\epsilon(E_0, t)$ is found from the equation

$$\int_{\epsilon(E_0, t)}^{E_0} dE / \beta(E) = t. \quad (\text{B3})$$

Notice that Eq. (B2) can be rewritten as:

$$\eta(E, t) = \delta(E - \epsilon(E_0, t)) \exp \left[- \int_E^{E_0} dE' / \left(\lambda(E') \beta(E') \right) \right], \quad (\text{B4})$$

where $\eta(E, t)$ is the probability for a single muon to pass the path t without interaction of SEL type and then one can easily see that Eqs. (B3) and (B4) lead to the Eqs. (2.2) after the following substitutions which are necessary for a return to the notations of Sec. II:

$$E_0 \rightarrow E_1, \quad E \rightarrow E_2, \quad \lambda(E) \rightarrow \bar{L}(E), \quad \beta(E) \rightarrow [dE(E)/dx]_{CEL}, \quad t \rightarrow L.$$

-
- [1] G. T. Zatsepin and E. D. Mikhalech, J. Phys. Soc. Japan, **17**, Suppl. A – III, 356 (1962).
 - [2] K. Kobayakawa, Nuovo Cimento B **47**, 156 (1967).
 - [3] S. Hayakawa, *Cosmic Ray Physics – Nuclear and Astrophysical Aspects*, Interscience Monographs and Texts in Physics and Astronomy, Vol. XXII, edited by R. E. Marshak (University of Rochester, New York, 1969).
 - [4] E. Kiraly, P. Kiraly, and J. L. Osborn, J. Phys. A **5**, 444 (1972).
 - [5] A. Misaki and J. Nishimura, Uchuusen-Kenkyuu, **21**, 250 (1976).
 - [6] V. I. Gurentsov, G. T. Zatsepin, and E. D. Mikhalech, Yad. Fiz. **23**, 1001 (1976) [Sov. J. Nucl. Phys. **23**, 527 (1976)].
 - [7] Y. Minorikawa, T. Kitamura, and K. Kobayakawa, Nuovo Cimento C **4**, 471 (1981).
 - [8] E. V. Bugaev, V. A. Naumov, and S. I. Sinegovsky, Yad. Fiz. **41**, 383 (1985) [Sov. J. Nucl. Phys. **41**, 245 (1985)]; Izv. Akad. Nauk SSSR. Ser. Fiz. **49**, 1389 (1985) [Proc. of the Acad. of Sci. of the USSR. Phys. Ser. **49**, 146 (1985)].
 - [9] D. P. Bhattacharyya, Nuovo Cimento C **9**, 404 (1986).
 - [10] O. C. Allkofer and D. P. Bhattacharyya, Phys. Rev. D **34**, 1368 (1986).
 - [11] V. N. Bakatanov *et al.*, Yad. Fiz. **55**, 2107 (1992) [Sov. J. Nucl. Phys. **55**, 1169 (1992)].
 - [12] V. A. Naumov, S. I. Sinegovsky, and E. V. Bugaev, Yad. Fiz. **57** (1994) 439 [Physics of Atomic Nuclei **57** (1994) 412].
 - [13] E. V. Bugaev *et al.*, Phys. Rev. D **58**, 054001 (1998); see also hep-ph/9803488 for more details and references.
 - [14] P. J. Hayman, N. S. Palmer, and A. W. Wolfendale, Proc. Roy. Soc. (London) **A275**, 391 (1963).
 - [15] J. L. Osborn, A. W. Wolfendale, and E. C. M. Young, J. Phys. A **1**, 55 (1968).
 - [16] L. Bergamasco and P. Picchi, Nuovo Cimento B **3**, 134 (1971).
 - [17] Yu. N. Vavilov, Yu. A. Trubkin, and V. M. Fedorov, Yad. Fiz. **18**, 884 (1974) [Sov. J. Nucl. Phys. **18**, 434 (1974)].
 - [18] N. Takahashi *et al.*, Uchuusen-Kenkyuu, **28**, 120 (1984).
 - [19] W. Lohmann, R. Kopp, and R. Voss, CERN Report No. 85-03, 1985 (unpublished).
 - [20] J. N. Capdevielle *et al.*, J. Phys. G **11**, 565 (1985).
 - [21] H. Bilokon *et al.*, Nucl. Instrum. Methods **A303**, 381 (1991).
 - [22] P. Lipari and T. Stanev, Phys. Rev. D **44**, 3543 (1991).
 - [23] K. Mitsui, Phys. Rev. D **45**, 3051 (1992).
 - [24] P. Antonioli *et al.*, Astropart. Phys. **7**, 357 (1997); V. A. Kudryavtsev *et al.*, Phys. Lett. B **471**, 251 (1999).
 - [25] A. A. Lagutin, P. B. Togobitsky, and A. Misaki, Izv. Altayskogo Gos. Universiteta **Special issue**, 93 (1998).
 - [26] W. Rhode and C. Cârloganu, in *Proceedings of the Workshop on Simulation and Analysis Methods for Large Neutrino Telescopes, Zeuthen, 1998*, edited by C. Spiering (DESY Zeuthen, Zeuthen, 1998), p. 247.
 - [27] Ch. Spiering and I. Sokalski (eds.), Baikal Collaboration Report No. 92/11, 1992; Baikal Collaboration, V. A. Balkanov *et al.*, Nucl. Phys. Proc. Suppl. **87**, 405 (2000).
 - [28] S. Barwick *et al.*, Wisconsin University Report No. MAD-PH-629, 1991; E. Andres *et al.*, Astropart. Phys. **13**, 1 (2000).
 - [29] E. Aslanides *et al.*, astro-ph/9907432; P. Amram *et al.*, Nucl. Phys. Proc. Suppl. **75A**, 415 (1999).
 - [30] L. K. Resvanis *et al.*, Nucl. Phys. Proc. Suppl. **35**, 294 (1994); S. Bottai *et al.*, Nucl. Phys. Proc. Suppl. **85**, 153 (2000).
 - [31] E. V. Bugaev, I. A. Sokalski, and S. I. Klimushin, hep-ph/0010323.
 - [32] R. P. Kokoulin, A. A. Petrukhin, in *Proceedings of the 22nd International Cosmic Ray Conference, Dublin, 1991*, edited by M. Cawley *et al.* (The Dublin Institute for Advanced Studies, Dublin, 1991), Vol. **4**, p. 536; R. P. Kokoulin, Nucl. Phys. B (Proc. Suppl.) **70**, 475 (1999).
 - [33] S. I. Klimushin, E. V. Bugaev, and I. A. Sokalski, Phys. Rev. D **64**, 014016 (2001) [hep-ph/0012032].
 - [34] T. K. Gaisser, *Cosmic Rays and Particle Physics* (Cambridge University Press, Cambridge, 1990).
 - [35] L. B. Bezrukov and E. V. Bugaev, Yad. Fiz. **32**, 1636 (1980) [Sov. J. Nucl. Phys. **32**, 847 (1980)]; *ibid.* **33**, 1195 (1981) [**33**, 635 (1981)].
 - [36] J. Breitweg *et al.*, Europ. Phys. J. **C7**, 609 (1999).
 - [37] L. V. Volkova, G. T. Zatsepin, and L. A. Kuzmichev, Yad. Fiz. **29**, 1252 (1979) [Sov. J. Nucl. Phys. **29**, 645 (1979)].
 - [38] S. Higashi *et al.*, Nuovo Cimento **43A**, 334 (1966).
 - [39] DUMAND Collaboration, J. Babson *et al.*, Phys. Rev. D **42**, 3613 (1990).
 - [40] A. Okada, Astroparticle Phys. **2** 393 (1994).
 - [41] S. Miyake, in *Proceedings of the 13th International Conference on Cosmic Rays, Denver, 1973*, (Colorado Associated Univ. Press, Boulder, 1973), Vol. **5**, p. 3638.
 - [42] MACRO Collaboration, M. Ambrosio *et al.*, Phys. Rev. D **52**, 3793 (1995).
 - [43] V. M. Fedorov *et al.*, in *Proceedings of the 19th International Cosmic Ray Conference, La Jolla, 1985*, edited by F. C. Jones, J. Adams and G. M. Mason (NASA Conf. Publ. 2376) (Goddard Space Flight Center, Greenbelt, MD, 1985), Vol. **8**, p. 39.
 - [44] Yu. N. Vavilov *et al.*, Bull. Acad. Sci. of the USSR, Phys. Ser. **34**, 1759 (1970).
 - [45] V. A. Kudryavtsev (private communication, August 2000).
 - [46] L. B. Bezrukov and E. V. Bugaev, in *Proceedings of the 17th International Cosmic Ray Conference, Paris, 1981* (Section

- d'Astrophysique, Centre d'Études Nucléaires de Saclay, Gif-sur-Yvette Cedex, 1981), Vol. **7**, p. 102; Yu. M. Andreev, L. B. Bezrukov, and E. V. Bugaev, *Yad. Fiz.* **57**, 2146 (1994) [*Phys. At. Nucl.* **57**, 2066 (1994)].
- [47] S. R. Kelner, R. P. Kokoulin, and A. A. Petrukhin, Moscow Engineering Physics Inst. Preprint No. 024-95, 1995; S. R. Kelner, R. P. Kokoulin, A. A. Petrukhin, *Yad. Fiz.* **60**, 576 (1997) [*Phys. At. Nucl.* **60**, 657 (1997)].
 - [48] R. P. Kokoulin kindly granted us in November, 1999 routines which had been written by him to compute muon cross sections. Some part of these routines are used in the MUM code.
 - [49] R. P. Kokoulin and A. A. Petrukhin, in *Proceedings of the 11th International Cosmic Ray Conference, Budapest, 1969*, edited by T. Gémsey *et al.* [*Acta Phys. Acad. Sci. Hung.* **29**, Suppl. 4, 277 (1970)]; R. P. Kokoulin and A. A. Petrukhin, in *Proceedings of the 12th International Cosmic Ray Conference, Hobart, 1971*, edited by A. G. Fenton and K. B. Fenton (University of Tasmania Press, Hobart, 1971), Vol. **6**, p. A 2436.
 - [50] S. R. Kelner, R. P. Kokoulin, and A. A. Petrukhin, *Yad. Fiz.* **62**, 2042 (1999) [*Phys. Atom. Nucl.* **62**, 1894 (1999)].
 - [51] S. R. Kelner, Moscow Engineering Physics Inst. Preprint No. 016-97, 1997.
 - [52] R. M. Sternheimer, *Phys. Rev.* **103**, 511 (1956); R. M. Sternheimer and R. F. Peierls, *Phys. Rev. B* **3**, 3681 (1971); R. M. Sternheimer, M. J. Berger, and S. M. Seltzer, *Atomic Data and Nuclear Data Tables*, **30**, 261 (1984).